ABSTRACT

Title of Thesis: AN INVESTIGATION ON THERMAL CHARACTERISTICS OF PREMIXED COUNTERFLOW FLAMES USING MICRO-THERMOCOUPLES

Roya Ghoddoussi, Master of Science, 2005

Thesis directed by: Professor André W. Marshall
Department of Fire Protection Engineering

Hydrogen addition is known to improve the stability of highly strained hydrocarbon premixed flames. Since the flame temperature is an important factor associated with extinction, it is of interest to study the thermal characteristics of the hydrogen-doped flames near extinction. Temperature profiles of highly strained lean-premixed pure CH_4 and CH_4/H_2 flames were measured in a counterflow configuration at strain rates far from and close to extinction. Point temperature measurements were made utilizing a micro-thermocouple probe. To improve the measurements, the thermocouple support design was enhanced and corrections were made for measurement errors where appropriate. Trends observed in experimental and modeling temperature profiles with changes in fuel composition and strain rate, agree favorably. However, there are some discrepancies between the measured and predicted absolute temperatures. Factors contributing to these discrepancies and the methods to reduce the thermocouple measurement errors are discussed.

AN INVESTIGATION ON THERMAL CHARACTERISTICS OF PREMIXED COUNTERFLOW FLAMES USING MICRO-THERMOCOUPLES

By

Roya Ghoddoussi

Thesis submitted to the Faculty of the Graduate School of the
University of Maryland, College Park in partial fulfillment
of the requirements for the degree of
Master of Science
2005

Advisory Committee:

Professor André W. Marshall, Chair/Advisor
Professor Gregory S. Jackson
Professor Arnaud Trouvé

Acknowledgements

First, I would like to express my deep gratitude to my research advisor Professor André Marshall for his continuous assistance, guidance, and support throughout this research project. With his positive attitude and infinite patience, he has always been there to guide and help me. I am especially thankful to Professor Gregory Jackson, my co-advisor for his insightful comments, guidance and encouragement. I would also like to thank the other member of my thesis committee, Professor Arnaud Trouvé for generous dedication of his time. Special thanks to Professor Kenneth Kiger for graciously allowing me to share his lab space and equipment. I am very thankful to Joseph Plaia, for kindly providing the numerical modeling data used in this work, and for responding to my numerous emails and questions, and also to Roxanna Sai for teaching me how to work with the experimental set-up and sharing her experiences with me. I would like to thank members of Fire Flow Research group for their friendship, assistance, and guidance throughout my studies and research. I would also like to thank the Chair, faculty and staff of the Department of Fire Protection Engineering for providing a friendly educational environment and making the experience of these past years at the University of Maryland an enjoyable one.

My special thanks to my parents and my brother, my role models, for their words of encouragement and their belief in me. Lastly but most importantly, my deepest appreciation and love goes to my husband Alireza Modafe for his encouragement, support, and assistance through all the steps of this journey. I thank him from the bottom of my heart.

Table of Contents

Acknowledgements ii

Table of Contents iii

List of Tables v

List of Figures vi

Chapter 1: Introduction 1
- 1.1 Overview 1
- 1.2 Literature Review 3
- 1.3 Objectives of Study 12

Chapter 2: Approach 13
- 2.1 Introduction 13
- 2.2 Experimental Test Facility 13
  - 2.2.1 Test Rig 13
  - 2.2.2 Traverse 15
- 2.3 Diagnostics 17
  - 2.3.1 Thermocouple Support Design 17
  - 2.3.2 Thermocouple Coating 20
  - 2.3.3 Data Acquisition System 21
- 2.4 Temperature Measurement Methodology 22

Chapter 3: Data Analysis 24
- 3.1 Introduction 24
- 3.2 Thermocouple Probe Heat Transfer 25
  - 3.2.1 Convection 25
  - 3.2.2 Conduction 29
  - 3.2.3 Radiation 33
  - 3.2.4 Catalysis 38
- 3.3 Non-uniform Thermocouple Heating 39
- 3.4 Thermocouple Positioning 40
- 3.5 Probe-induced Disturbances 41
- 3.6 Thermal Inertia 42
- 3.7 Measurement Validation 49
  - 3.7.1 Model Quality Assessment 49
  - 3.7.2 Uncertainty in Experimental Parameters 50

Chapter 4: Results 53
- 4.1 Introduction 53
- 4.2 Steady Flames 53
  - 4.2.1 Effects of Strain 53
  - 4.2.2 Effects of Fuel 57

4.3 Oscillating Flames 60

Chapter 5: Conclusions 64

Appendix A: Illustration of National Instruments LabVIEW Program Utilized for Temperature Measurement and Traverse Control 66

Appendix B: Error Analysis for Steady-State Thermocouple Measurements 71

Bibliography 73

List of Tables

4.1 Measured and adiabatic CH_4 flame temperature 56

4.2 Flame width and temperature gradient 57

List of Figures

1.1 Premixed methane/air flame structure ($\phi = 0.65$, $\kappa_{mean} / \kappa_{ext} = 0.8$).....3

1.2 Counterflow premixed flame 4

2.1 Rig set-up.....14

2.2 Experimental set-up for temperature measurement 16

2.3 Thermocouple support 17

2.4 Thermocouple wire expansion in flame.....18

2.5 Thermocouple single support design 18

2.6 Measurement of thermocouple support temperature 20

2.7 Thermocouple coating microscopic images.....21

3.1 Heat transfer modes in thermocouple 25

3.2 Calculated Nusselt numbers at a 900 K near flame location (Methane flame of $\phi = 0.65$ and $\kappa_{mean} / \kappa_{ext} = 0.8$) 27

3.3 Variation of conduction cooling error with thermocouple wire length in methane flame ($\phi = 0.65$, $\alpha = 0.1$ and $\kappa_{mean} / \kappa_{ext} = 0.6$).....30

3.4 Variation of conduction heating error with thermocouple wire length in methane flame ($\phi = 0.65$, $\alpha = 0.1$ and $\kappa_{mean} / \kappa_{ext} = 0.6$) 31

3.5 Temperature difference between thermocouple and support.....32

3.6 Calculated radiation correction using Nusselt number correlations at a 900 K near flame location (Methane flame of $\phi = 0.65$ and $\kappa_{mean} / \kappa_{ext} = 0.8$) 35

3.7 Effect of thermocouple wire diameter on the radiation loss (Methane flame of $\phi = 0.65$ and $\kappa_{mean} / \kappa_{ext} = 0.8$).....37

3.8 Probe induced disturbances.....41

3.9 Average temperature decay for calculation of the time constant.....43

3.10 Experimental set-up for measuring response time of the probe 45

3.11 100 ms of uncompensated and compensated sinusoidal signal at τ = 15 ms 47

3.12 100 ms of uncompensated and compensated sinusoidal signal at τ = 30 ms 48

3.13 Comparison between computed profiles and Raman scattering temperature profiles (Case C, $\kappa_{mean} / \kappa_{ext} = 0.5$, $\kappa_{ext} = 400\ s^{-1}$) 50

3.14 Uncertainty in experimental conditions **(a)** Spherical bead geometry **(b)** Cylindrical bead geometry 52

4.1 Effect of strain on CH_4 flames – Measurement results (ϕ = 0.65) **(a)** α = 0.00 **(b)** α = 0.05 **(c)** α = 0.10 54

4.2 Effect of strain on CH_4 flames – Modeling results (ϕ = 0.65) **(a)** α = 0.00 **(b)** α = 0.05 **(c)** α = 0.10 55

4.3 Effect of H_2 addition on CH_4 flames – Measurement results (ϕ = 0.65) **(a)** 60% of κ_{ext} **(b)** CH_4 at 80% and CH_4/H_2 at 85% of κ_{ext} 58

4.4 Effect of H_2 addition on CH_4 flames – Modeling results (ϕ = 0.65) **(a)** 60% of κ_{ext} **(b)** CH_4 at 80% and CH_4/H_2 at 85% of κ_{ext} 59

4.5 Changes in the flame temperature as a function of strain rate for CH_4 and C_3H_8. Extinction occurs at tip of the knee of the profiles 60

4.6 Uncompensated and compensated temperature signatures in the methane flame brush (ϕ = 0.65, α = 0.0, $u'/u_{mean} = 0.15$) 61

4.7 Measured and calculated (a) mean and (b) fluctuating temperature profiles for ϕ = 0.65, $\kappa_{mean} / \kappa_{ext} = 0.9$, T_{in} = 300 °C for (Δ - α = 0.10, $u'/u_{mean} = 0.0$), (○- α = 0.10, $u'/u_{mean} = 0.03$) 62

Chapter 1: Introduction

1.1 Overview

Many practical combustion systems such as gas turbines, boilers, and internal combustion (IC) engines operate with lean premixed flames to limit combustion temperatures and associated NO_x emissions. The NO_x formation rate increases exponentially with temperature. By lowering the fuel equivalence ratio, the flame temperature is lowered, and as a result NO_x emissions are reduced [1]. However, lowering the fuel equivalence ratio also lowers the flame stability, which may lead to local flame extinction and increase in CO emission. The flame stability depends on the competition of heat production from exothermic chemical reactions in flame and heat loss due to radiation and diffusion. It has been found that addition of small amount of hydrogen can improve the stability of lean premixed flames because of the higher flame speed and wider flammability limits of hydrogen. Addition of H_2 to the fuel increases the flame speed, leading to faster transportation of species and faster reactions. In addition, wide flammability limits of hydrogen supports combustion of very lean mixtures [2]. Therefore, the hydrogen-doped flame can be stabilized at lower flame temperatures, allowing a reduction in NO_x and CO emissions [3].

In most practical combustion systems the nature of the flow is turbulent. Under many practical conditions the turbulence can be thought to wrinkle and deform the flame front [1]. In the wrinkled flamelet regime, turbulent flames can be modeled as a set of stretched laminar flamelets [4]. Therefore, the results obtained from studying stretched laminar premixed flames improve the capability to characterize the combustion processes occurring in turbulent reacting flows.

The flame temperature is one of the most important variables in characterizing flames and also in determining local heat release and reaction rates in flames. Moreover, many of the parameters such as flame speed and thickness that are used to analyze flames are temperature dependent [1]. Therefore studying the temperature signature of laminar stretched flames can provide valuable information for modeling turbulent premixed flames leading to improvement in design of practical combustion systems.

1.2 Literature Review

The flame generated from a premixed fuel-oxidizer system is called a premixed flame. If the equivalence ratio for such a system is less than one, meaning there is an excess of oxidant present in the mixture, the flame is said to be lean. Structure of a one-dimensional premixed methane flame, normal to the flame front is shown in Figure 1.1. The data has been obtained from an already developed 1-D computational model [5].

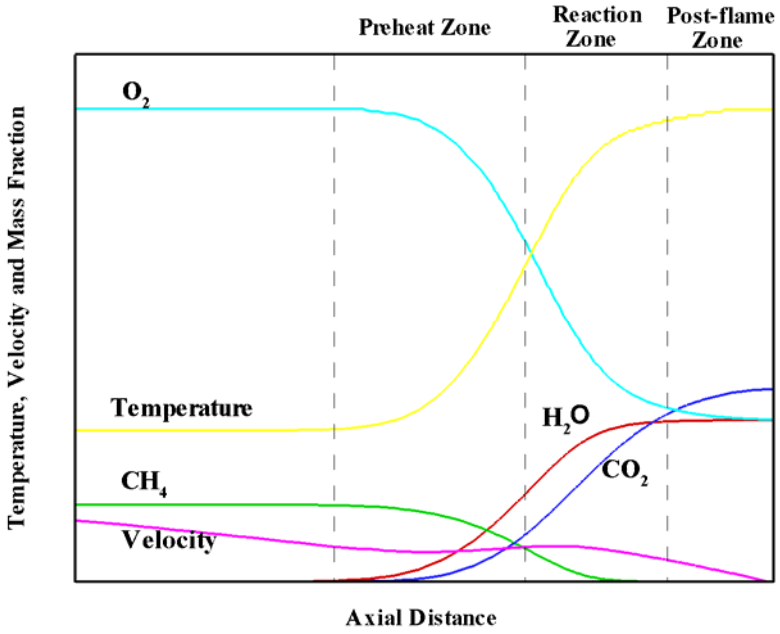

Fig. 1.1: Premixed methane/air flame structure ($\phi = 0.65$, $\kappa_{mean} / \kappa_{ext} = 0.8$)

The flame is considered to be divided into three zones: a preheat zone, a reaction zone, and a post-flame zone [6]. In the preheat zone the unburned gases approaching the flame are heated up by the diffused heat from the reaction zone. However, due to the presence of convective flow, the increase in the temperature profile is not linear [7]. The majority of exothermic chemical reactions occur in the

reaction zone, where the gas temperature has reached the ignition temperature. The reaction zone is typically less than 1 mm wide. Thus, the gradients of temperature and species concentration are very large. These large gradients facilitate diffusion of heat and radical species to the preheat zone and sustain the flame [1]. In the post flame zone some exothermic radical recombination reactions take place. However, the radical concentration is too low to have much effect on the temperature profile.

The counterflow flame configuration is commonly used to study the behavior of stretched flames. This flame can be produced from impinging two streams of coaxially opposed combustible mixture (Figure 1.2). At high strain rates the twin counterflow flames are pushed to the stagnation plane to keep the balance between the flame speed and the flow velocity. At these conditions the classic double flame counterflow structure merge and appear as a single flat and symmetrical flame at the stagnation plane.

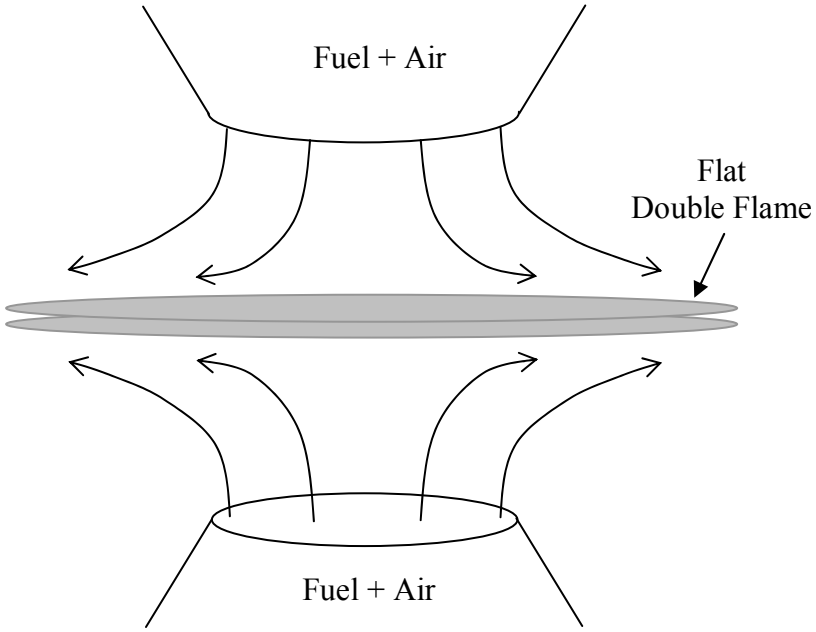

Fig. 1.2: Counterflow premixed flame

Counterflow flames are of fundamental research interest since at the centerline of the nozzles gradients only exist in the axial direction and the flow can be regarded as one-dimensional. Also, as a result of the symmetry of the flow and minimum heat loss, counterflow system provides a nearly adiabatic stagnation flame [8]. Another benefit is the ability to control and study the effect of positive stretch on the structure of the flame. Opposed flow configurations are also used to examine the influence of fuel type, equivalence ratio, bulk strain and imposed oscillations on extinction [9]. As mentioned in § 1.1, the results of such studies can be applied in modeling turbulent premixed flames.

Flame stretch ($\dot{s}$) is defined as the time rate of change of flame area (A) per unit area [4].

$$\dot{s} = \frac{1}{A}\frac{dA}{dt} \tag{1.1}$$

Flame stretch is identified with two physical processes: strain rate (κ) and propagation of curved flame [4]. For the stationary planar flame in the stagnation flow, flame stretch and strain rate are identical and characterized by the local velocity gradient just upstream of the flame [7,10].

$$\kappa = -\frac{du}{dx} \tag{1.2}$$

Flame response to stretch depends critically on the rate of heat to mass diffusivity. This response has been found to be especially important for mixtures with unequal heat and mass diffusivities ($Le \neq 1$). Lewis number, $Le = \alpha / D$, represents the ratio of thermal diffusivity, α, to mass diffusivity of the deficient component, D, which for the lean premixed flames is the fuel. Besides preferential

diffusion (Lewis number effect), stability and extinction limits of stretched premixed flames depend on the mixture equivalence ratio, stretch rate and downstream heat loss [11,12]. Several studies [10,13-15] have concluded that the kinetic mechanism is the cause of extinction. It has been found that for most hydrocarbon/air flames regardless of the flame type and flow configuration, the limiting temperature, below which the chain terminating reaction $H + O_2 + M \rightarrow HO_2 + M$ dominates over the chain branching reaction $H + O_2 \rightarrow OH + O$ is about 1200 °C to 1300 °C. At this condition, the combustion will slow down, and eventually flame can no longer exist.

According to Law et al. [8], for a diffusionally neutral flame (*Le* = 1), increase in stretch will push the flame closer to the stagnation surface to keep the balance between the flame speed and the flow velocity. This will produce a thinner flame, reduce the residence time, and cause incomplete chemical reactions and eventual extinction. Thus for such flames the extinction is a result of stretch-induced incomplete reactions.

For a flame with a *Le* < 1, where the deficient reactant is the more mobile one, an increase in the stretch rate will primarily increase the deficient component flux to the flame, thus raising the maximum flame temperature. As the stretch rate increases the flame is pushed closer to the stagnation surface. In this situation similar to *Le* = 1, there will be a reduction in the flame thickness [7]. Since downstream heat loss is assumed negligible for the counterflow premixed flames due to the close to adiabatic stagnation surface [11], the flame extinction can be associated with the combustion reactions that cannot be completed because of shorter residence time of the flow in the reaction zone [11,13,16]. The incomplete combustion lowers the temperature

below the limiting 1200 °C temperature, leading to flame extinction [15]. Although the extinction mechanism is similar to that of the $Le = 1$, the extinction of a $Le < 1$ flame will happen at higher stretch rates to make up for the higher flame temperatures initially attained [8].

In the case of $Le > 1$, where the leaner reactant is the less diffusive one and the upstream heat loss exceeds mass gain, increasing the stretch rate will reduce the flame temperature. Contrary to the $Le < 1$ flame, the deficient reactant will be totally consumed crossing the flame [8]. In such flames the extinction occurs at a finite distance from the stagnation surface due to flame stretch [16]. Overall it appears that temperature drop below the limit temperature is responsible for the flame extinction regardless of it being due to incomplete reaction or stretch.

Lean premixed methane flames have Lewis numbers in the range of $0.9 < Le < 1.0$. Lean hydrogen/air flames, on the other hand, have Lewis numbers in a lower range ($0.25 < Le < 0.3$) [17]. Therefore, adding hydrogen to methane/air mixture will decrease the effective fuel Lewis number. This reduction in average Lewis number will increase the maximum strain rate before extinction temperatures are reached. Due to relatively small activation energy of hydrogen compared to hydrocarbon fuels, radical concentrations are increased significantly with hydrogen addition in strained flames [3]. Since the thermal and mass diffusivities of hydrogen are much greater than the hydrocarbon fuels, adding H_2 to methane also increases the flame speed, leading to faster transportation of species and faster reactions. As a result the combustion efficiency at higher strain rates can be improved under proper conditions with increasing strains [18].

Since in most practical combustion systems the flame is exposed to turbulence and unsteadiness, influence of oscillations on the flame structure and extinction should also be investigated. The frequency and amplitude of the oscillations are the two parameters that characterize this effect [7]. According to Sardi et al. [19], flame extinction under periodic oscillations depends on the duration of imposed oscillations. In other words, the flame may persist under oscillations even if the instantaneous strain rates surpass steady state extinction strain rates temporarily. Exceeding the critical strain rates may initiate flame extinction but will not be completed unless the gradual cooling of the reaction zone during local quenching at high strain region of the oscillation cycle forces the temperature below the limiting temperature. In this situation the re-ignition of the flame and increase in the temperature that occurs during low strain rate part of the oscillation cycle can no longer happen, leading to flame extinction.

Flame temperature is a key feature for analyzing flame structure, since most of the flame parameters such as flame velocity, thickness and extinction are temperature dependent [1]. Although a large number of computational studies have been conducted for strained flames, insufficient amount of high accuracy experimental temperature data is available to verify these models. Several techniques have been utilized to measure counterflow flame temperature.

Logue [20] used thin filament pyrometry, a visual spectrum technique to measure temperature in a low strain stagnation diffusion flame near extinction. A 15-μm silicon carbide fiber with nearly constant emissivity and small axial conductivity was positioned normal to the flame surface. The flame temperature was determined

by relating the fiber luminescence, captured by a CCD digital camera, into a temperature that was used to determine the gas temperature.

Temperature measurement in a near-stoichiometric methane/air mixture by Law et al. [21] were derived from the shape of Raman spectrum and by fitting the measured spectrum to a theoretical spectrum at a known temperature. Non-intrusive, optical temperature measurement techniques have many advantages but they are usually costly and require a lot of expertise in their operation. Thermocouples are traditionally used to determine gas temperatures in the flames. In fact, temperature profiles from other techniques such as Raman scattering are validated by comparing with the results from thermocouples measurements [22]. Thermocouples are low cost, easy to use, and high precision tools for measuring spatial and temporal temperature profiles.

Tsuji et al. [16] measured temperature distributions across lean and rich near extinction counterflow premixed flames of methane/air and propane/air to investigate the extinction mechanism of such flames. The temperature distributions were measured with a 0.05 mm silica-coated Pt / Pt 13% Rh thermocouple. Flame temperature of lean methane/air had a slight increase as the velocity gradient was increased and then decreased as the flame approached extinction limit. Flame temperature of rich methane/air on the other hand, seemed to be almost independent of the velocity gradient except near the extinction limit. Propane/air showed reverse behavior in comparison with methane/air when the velocity gradient was increased.

Sato [13] used a silica-coated Pt-20% Rh / Pt-40% Rh thermocouple of 0.1 mm wire diameter to measure the temperature and investigate extinction behavior of

premixed stagnation flames of methane/air, propane/air and butane/air with a variety of Lewis numbers. The thermocouple was positioned parallel to the flame to minimize the conduction heat losses. Similar to Tsuji et al. [16] findings, opposite situations were observed between lean and rich flames of these fuels. The studies of Sato [13] and Tsuji [16] seem to be more focused on the behavior of flame and pattern of changes in its temperature as the flame approaches extinction than measuring the true flame temperature. No corrections were made for the thermocouple radiation losses in either of these studies.

A 50-μm Pt / Pt 10% Rh thermocouple was used by Smooke [23], to measure temperature profile in counterflow methane/air diffusion flame. The thermocouple was coated with a layer of yttrium oxide to avoid catalytic effects. The results from radiation corrected temperature measurements were compared with the computational values. The discrepancy in profiles was attributed to the uncertainties in the computational model.

Korusoy [15] measured the temperature along the stagnation plane with a bare 50-μm Pt / Pt 13% Rh thermocouple to study the effects of equivalence ratio, bulk velocity and nozzle separation on the extinction and re-ignition of the lean premixed opposed methane-air flame. Under-estimation of the temperature caused by thermocouple radiation was assumed to be mostly compensated by the thermocouple catalytic effects. Therefore the uncertainties in the absolute temperature values were considered to be less than 3% of the mean, not affecting the observed trends. Korusoy verified the extinction temperature acquired from a bare thermocouple by

comparing it to the value reported by Sato [13] obtained from a coated thermocouple with no radiation corrections.

The instantaneous temperature traces by Luff et al. [9], in lean premixed counterflow flames of air and methane, propane and ethylene were measured using 25-μm type R thermocouples. To reduce the catalysis effects a protective quartz coating was applied on the thermocouples. The temperature traces were measured at the stagnation point to study the temporal decay of flame temperature during forced oscillations. Local extinction and re-ignition was observed by lowering the equivalence ratio, which could also be observed following the fluctuations in the temporal decay curves before complete extinction.

Most of the previous studies on the extinction and stability of stretched premixed flames were based on single component fuels. Although practical combustion systems use multi-component fuels, few studies have been conducted on the thermal characteristics and behavior of multi-component fuels in strained lean premixed flames. The present study will provide experimental temperature data on highly strained lean premixed methane/air flames, with and without hydrogen addition. Measurement of temperatures in hydrogen-doped flames is especially challenging because of the catalytic oxidation of H_2 on the thermocouple surface and the errors that it will cause.

1.3 Objectives of Study

The goal of this study is to improve the understanding of lean premixed flame behavior at high strain rates and close to extinction. Influence of hydrogen addition on stability of lean hydrocarbon flames near extinction is evaluated. In particular the effect of strain and its fluctuations on temperature profiles at conditions far and close to extinction is studied. A platinum based micro-thermocouple was utilized for temperature measurements. Thermocouple catalysis errors in these reducing flames were lowered by coating the thermocouples. Radiation and conduction errors were analyzed and in the case of preliminary study on oscillating flames, the temperature measurements were compensated for thermal inertia. In addition experimental results were compared to the predictions from an already developed reduced chemistry model [5].

Chapter 2: Approach

2.1 Introduction

The temperature measurements to characterize the counterflow premixed flames in this study were carried out along the centerline of the counterflow nozzles, utilizing coated type R micro-thermocouples. This chapter begins with the experimental procedures used, including the experimental setup, diagnostics, and the measurement methodology. Then it is followed by discussion of the data analysis method used to derive the real gas temperature from raw thermocouple data, and the measures taken to reduce the errors.

2.2 Experimental Test Facility

2.2.1 Test Rig

The counterflow flame temperature measurements were performed in a set-up developed by Yubin Cong [24] and improved by Roxanna Sai [25] at earlier stages of this project. The experimental rig set-up consists of two identical nozzles positioned in a vertical opposed flow configuration (Figure 2.1). The nozzle exit diameters are 8.5 mm and the nozzle separation distance is 0.7 ± 0.01 mm. Electronic mass flow controllers adjust total hydrocarbon fuel, total hydrogen, and individual air flow through the top and bottom nozzles. Identical rotameters downstream of fuel and hydrogen mass flow controllers split the flow and send equal amounts of fuel and hydrogen to each nozzle. Electric air pre-heaters are utilized to elevate nozzle exit flow temperature up to 300°C. The higher initial temperatures before combustion

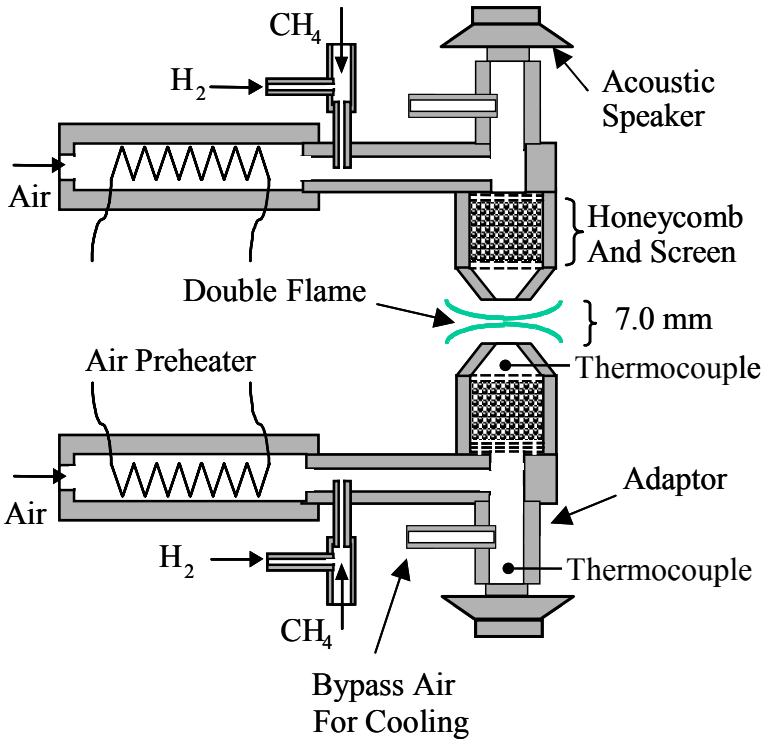

Fig. 2.1: Rig set-up

provide more stability at leaner flame mixtures and higher nozzle exit velocities. Nozzle exit temperatures are measured by thermocouples positioned in honeycomb flow straighteners just upstream of the nozzles. The honeycomb enhances fuel and air mixing and reduces variations in velocity and temperature across the nozzle before the flow exits.

Two speakers with a maximum input power of 60 Watts are placed upstream of nozzle exits as illustrated in figure 2.1. The speakers are driven by a function generator and an amplifier. The function generator provides a sinusoidal signal of the desired frequency to the amplifier. When supplied with an amplified sinusoidal voltage, the speakers impose oscillations in upstream nozzle pressure and thus nozzle exit velocities. This flow oscillation, results in a sinusoidal variation in the stagnation flame temperature. A multi-meter is employed to measure the input voltage to the

speakers. An empirically derived relation correlates the input voltage of the speakers to the amplitude of velocity oscillations at the nozzle exit [5]. Small amount of cool air that bypasses the heaters is bled into the speaker plenum to maintain the speakers within their service temperature range.

A National Instruments (NI) data acquisition system is utilized to control the burner operations. The user can specify the equivalence ratio, ϕ, the fraction of oxygen consumed by hydrogen, α, and the desired nozzle exit velocity through a NI LabVIEW program developed for interfacing with the data acquisition board. For the mixtures ϕ is defined by the fraction of oxygen consumed by both fuel components combined. The analog output of the data acquisition board sends an appropriate signal to the mass flow controllers to set the desired flow rate and composition. The nozzles exit flow temperatures are also measured and displayed so that the user can adjust the temperatures by changing the voltage supplied to the air preheaters.

2.2.2 Traverse

An XYZ traverse system was used to obtain accurate positioning and incremental movement of the temperature probe. The positioning system in the X direction was utilized to move the probe horizontally out of the rig before lighting the flame and to return the probe back to the exact previous location between the nozzles for repeatability of the experiments. For temperature measurements at different locations along the centerline of the nozzles, the positioning system at Z direction was employed to shift the probe vertically. The traverse in the Y direction was used to adjust the position of the probe at the centerline of the nozzles. Velmex positioning

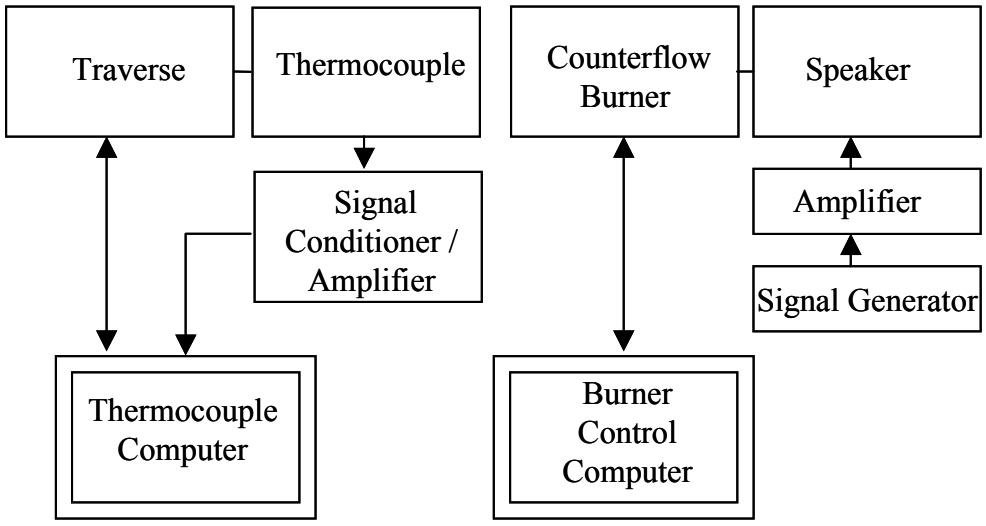

Fig. 2.2: Experimental set-up for temperature measurement

systems (MA2509Q1-S2.5 and MA1503Q1-S1.5) in the X and Z directions were equipped with stepping motors that could move the probe to a target position with a 10μm resolution.

The stepping motors were controlled by a Velmex VXM-2 programmable stepping motor controller. The stepping motor controller could either be operated as stand alone via the jog buttons on the front panel or run interactively from the computer through a custom developed National Instruments LabVIEW program (Appendix A) to set the control variables of the stepping motors such as: moving direction, motor speed, motor position, zeroing motor position and the capability to switch between stand-alone or interactive controller operation. The LabVIEW program sends commands in the format of ASCII characters to the controller through the RS-232 interface and displays the indexing feedback from the controller. Figure 2.2 illustrates the experimental set-up for the temperature measurement.

2.3 Diagnostics

2.3.1 Thermocouple Support Design

Instantaneous local temperatures were measured using a type R (Pt/Pt–13%Rh) thermocouple of 50 μm wire diameter with a bead of approximately 100 μm in diameter. The high melting point of type R thermocouple (2023 K) makes it a suitable probe for the range of temperatures in this study and the small size of the probe provides high resolution with minimal disturbance of the flame. Low response time and reduction in the radiation losses are other benefits of the small size of the probe. As a preliminary design the thermocouple bead was suspended between two 0.8 mm diameter, single bore ceramic supports separated by 20 mm (Figure 2.3). The supports were fixed within a modified thermocouple connector. Since in this design a considerably long portion of the thermocouple wire was exposed to the surrounding environment, thermal expansion and bending of the thermocouple wire in the flame region caused uncertainties in defining the exact axial location of the bead.

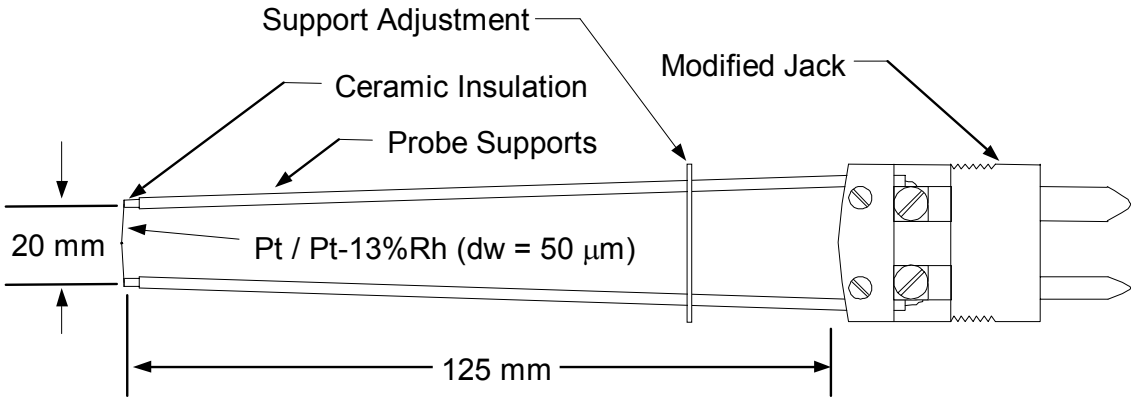

Fig. 2.3: Thermocouple support [27]

As shown in the snapshots in the figures 2.4.a to 2.4.c, when the thermocouple position changed from the cooler upstream region of flame to the high temperature flame region, the tightly drawn wire expanded and moved. In such condition the wire has a low tensile strength and pulling the wire, as an effort to straighten it, will only cause the wire to break. As a result a change in the support design was necessary.

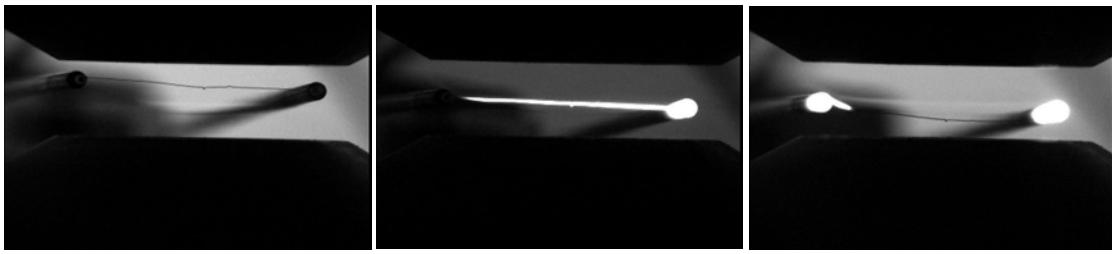

(a) (b) (c)

Fig. 2.4: Thermocouple wire expansion in flame

In the new design a smaller length of thermocouple wire (~ 9 mm) was exposed. The exposed wire was shaped into a flat semicircular form. The remaining thermocouple wires were insulated within a single 1.1 mm diameter twin bore ceramic cylinder, which in turn was housed within a nickel alloy protective tube (Figure 2.5). Probe-induced perturbations are reduced in this single support design.

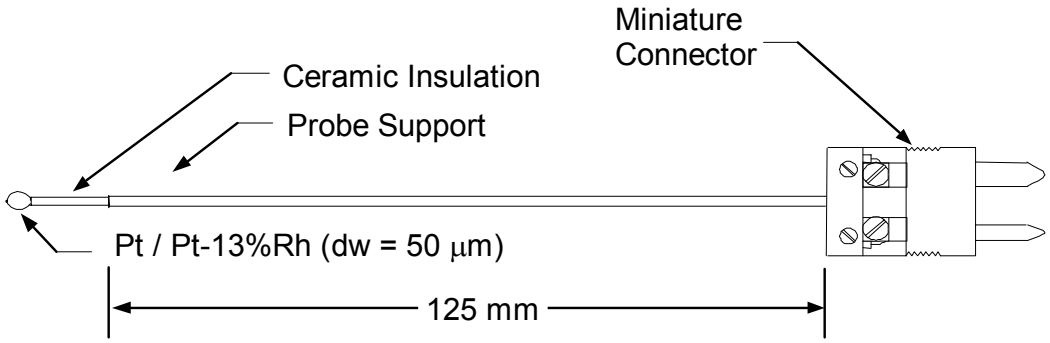

Fig. 2.5: Thermocouple single support design

Although in this design the shorter length of exposed wire significantly reduces thermocouple positioning errors caused by thermal expansion, conduction losses may not be negligible anymore. Ceramic insulation with much larger surface area than the exposed thermocouple wire loses more heat from radiation. As a result, the insulated section of the thermocouple wire has a lower temperature than the exposed part, which increases the heat conduction through the wires. Dependence of conduction heat loss on the length of the wire will be discussed in more details in § 3.2.2. To quantify and account for the conduction heat loss in deriving the gas temperature from the thermocouple bead temperature, the temperature of the insulated wire should be known.

A minor change in the thermocouple support design was made. In order to measure the insulated wire and the gas temperature simultaneously, a four-hole ceramic insulator of the same diameter was used to thread another thermocouple. The junction of this second thermocouple was attached to the support (Figure 2.6). The insulated wire temperature can be obtained from measuring the support temperature based on the assumption that the insulated wire is in full contact with the inner surface of the ceramic insulator tube all through its length. However, the measurement results proved the assumption of complete thermal contact of the insulated wire and support to be wrong since unexpectedly large temperature differences between the exposed and insulated wire, in the range of 600 – 700 degrees were observed. Through further investigation and calculations, conduction error was found to be negligible and the earlier single thermocouple design was used for the temperature measurements.

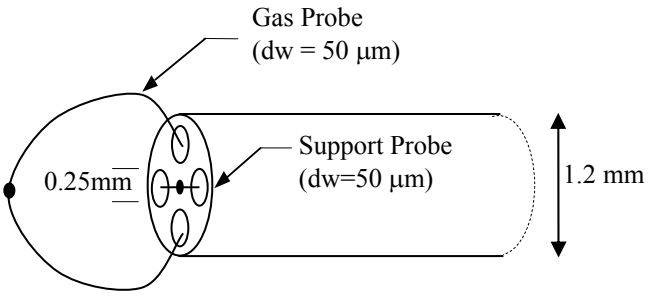

Fig. 2.6: Measurement of thermocouple support temperature

2.3.2 Thermocouple Coating

In this study, platinum-based type R thermocouples were used for temperature measurement due to their high service temperature. Catalytic reactions in reducing combustion environments will produce inaccuracies in platinum-based thermocouples temperature readings. In order to reduce this effect, a non-catalytic coating is applied on the thermocouple bead and wires. Some of the factors taken into account for choosing the coating were: having a similar thermal expansion coefficient as the wire to avoid cracking when exposed to heat, stability of the coating, and ease of application. In § 3.2.4 the catalytic effect will be discussed in more details.

Several types of coating were tested and Aremco Ceramabond 569-VFG gave the best results for our application. This aluminum oxide/potassium silicate coating was recommended by Burton et al. [26] as a non-toxic coating that lasts for several hours of use before degradation. According to the manufacturer, Ceramabond 569 adheres well to metals and can be used at temperatures as high as 1900 K. The best method to apply a thin layer of coating was found to be using a fine-tip brush. To make sure that the thermocouple bead and exposed surfaces of the wires were completely covered with the coating, the thermocouple was inspected using a high

magnification optical microscope (Figure 2.7). This inspection was done before and after exposure to heat to make sure that the coating performance was satisfactory. The coated thermocouple bead under different magnifications is pointed out with arrows in this figure. The coating increased the measurement junction diameter to 200 μm.

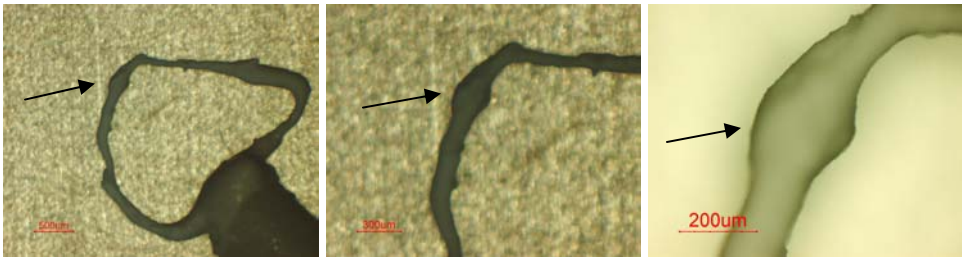

Fig. 2.7: Thermocouple coating microscopic images

2.3.3 Data Acquisition System

National Instruments 5B40-05 signal conditioner with a 10 kHz bandwidth was used to amplify the thermocouple millivolt signal by a factor of 100 and to filter the background electrical noise. The wide bandwidth makes the signal conditioner suitable for measuring signals that change rapidly with time. The amplified analog signal is interfaced to a 16 bit National Instrument PCI-MIO-16XE-50 data acquisition board and converted to digital data. The DAQ board is mounted within a PC running a custom National Instruments LabVIEW program (Appendix A). The program converts the digitized voltages to actual temperatures via a standard polynomial equation and displays the temperature signature for inspection before saving the data to disk. Moreover, the program provides statistical temperature data such as mean, minimum, maximum, and standard deviation. The data acquisition

parameters such as frequency and sampling time can be easily changed in the LabVIEW program control panel.

2.4 Temperature Measurement Methodology

Thermal behavior of close to extinction premixed flames of pure methane and hydrogen doped methane under both steady-state and oscillatory upstream velocities are investigated in this study. In order to consistently and accurately study the effects of strain and hydrogen doping on the thermal characteristics of methane flames, important parameters were determined. The experiment matrix was designed so that certain parameters were kept constant while effects of the other variables were evaluated.

The hydrogen doped mixtures are characterized by equivalence ratio, ϕ, defined as the fraction of O_2 consumed by both fuel components combined and by α, the fraction of O_2 consumed by H_2. The thermocouple service limit, imposed by its melting point was an important parameter in selection of ϕ and α. In the current study the mixture ϕ was kept constant at 0.65 and α ranged from 0.0 to 0.1, which was found to be adequate to observe impacts of H_2 on the methane flame [25].

The extinction strain rate is a function of equivalence ratio, fuel composition, and inlet temperature. In order to find the extinction strain rate of the steady flame, ϕ and α are kept unchanged. The velocity of the fuel and air combination leaving the nozzles with a 300°C exit temperature is slowly increased in 0.1 m/s increments after thirty seconds of stable operation. At the inlet velocity that the flame extinction occurs, the corresponding global strain rate, κ_{ext}, is obtained by dividing the mean exit

flow velocity by half of the separation distance between nozzles. Thermal behavior of the steady flame at $\kappa_{mean} / \kappa_{ext} = 0.85$ and $\kappa_{mean} / \kappa_{ext} = 0.6$ corresponding to close and far from extinction conditions respectively, was investigated for each fuel mixture.

Type R thermocouples of 50 μm wire diameter were used in pure methane and hydrogen-doped methane flames because of their high melting point (2023 K) [28]. The thermocouples were coated to minimize the catalytic effect. This coating increased the bead diameter to 200 μm. The temperatures were measured along the centerline of the nozzles with 0.25 mm increments at positions away from the flame and 0.125 mm increments at positions close to the flame. Exactly 10,000 data points separated by 1 ms were sampled at each position at the steady conditions and at the oscillating conditions 300,000 data points separated by 0.1 ms were sampled at each position.

Chapter 3: Data Analysis

3.1 Introduction

The temperature measured by the thermocouple may differ from the real gas temperature. There are several reasons for the difference. Radiation and conduction losses, thermal inertia, non-uniform thermocouple heating, catalytic effects, and the effect of probe intrusion on the flame are major factors affecting the reading of the thermocouple. The relative effect of these factors depends not only on the properties of the thermocouple itself, but also on the gas phase properties and whether the measurement is done at steady or transient condition. In order to derive a true gas temperature from the thermocouple measurement, a good understanding of all major sources of error is required. In this section various possible sources of errors encountered in thermocouple measurements and our approach to eliminate or minimize these errors are discussed.

Comparison of the experimental data with the results from an already developed computational model [5], the accuracy of which has been verified by comparison with a non-intrusive measurement temperature data from another source [21], helped us to get an estimate of the importance of some of the errors which could not be quantified otherwise. The model solves for flow velocity, temperature, and species mass fractions along the central axis of the flow within a cylindrically symmetric counterflow premixed flame. In § 3.7 more details about the validity of the model will be discussed.

3.2 Thermocouple Probe Heat Transfer

The energy balance on the thermocouple bead is a combination of convection, radiation, conduction heat transfer, and catalysis induced heating [22,27] as shown in figure 3.1. The energy balance on the thermocouple bead can be expressed as

$$\dot{Q}_{conv} + \dot{Q}_{rad} + \dot{Q}_{cond} + \dot{Q}_{cat} + \dot{Q}_{stor} = 0 \qquad (3.1)$$

where $\dot{Q}$ is the net rate of heat transfer. In the steady state conditions the rate of change of energy storage in the thermocouple, $\dot{Q}_{stor}$, is equal to zero. Since the purpose of using the thermocouple is measuring the local gas temperature, it is preferred to have convection as the major source of heat transfer to the thermocouple.

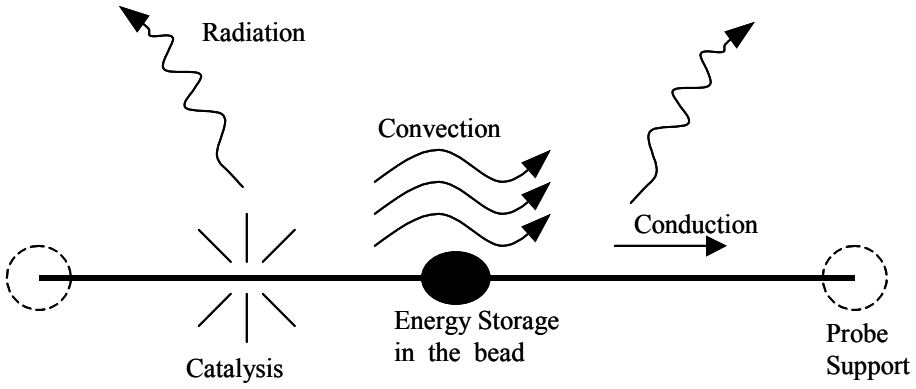

Fig. 3.1: Heat transfer modes in thermocouple

3.2.1 Convection

Modeling of the convective heat transfer around a thermocouple is not an easy task and involves some uncertainties. Selection of the appropriate correlation for calculation of the Nusselt number and estimation of the properties of the gas surrounding the thermocouple, especially its thermal conductivity are the two main

challenges for accurate modeling [22]. The heat gained by the thermocouple, at temperature T_b, is convected by the gas at T_g which, is described by:

$$\dot{Q}_{conv} = hA_s(T_g - T_b) \tag{3.2}$$

where, A_s is the bead surface area, and h is the convective heat transfer coefficient of the flow over the thermocouple junction defined as $h = kNu/d$. k is the thermal conductivity of the gas, Nu is the Nusselt number, and d is the bead diameter.

The Nusselt number correlation is usually chosen based on the thermocouple bead geometry, being spherical or cylindrical. The commonly used correlation for forced convection over a spherical geometry is proposed by Whitaker [29] for $3.5 < \mathrm{Re} < 76\times10^4$ and $0.71 < \mathrm{Pr} < 380$.

$$Nu_{d,sph} = 2.0 + \left(0.4\,\mathrm{Re}_d^{1/2} + 0.06\,\mathrm{Re}_d^{2/3}\right)\mathrm{Pr}^{0.4}\left(\mu_\infty/\mu_s\right)^{1/4} \tag{3.3}$$

The dimensionless groups in this equation are Reynolds number, $\mathrm{Re}_d = \rho u d/\mu$, and Prandtl number, $\mathrm{Pr} = \mu c_p/k$; where u is the velocity of flow over the thermocouple, and μ, ρ, and c_p denote the dynamic viscosity, density, and the specific heat of the gas. All properties except the dynamic viscosity at surface, μ_s, are evaluated at T_∞. Ranz and Marshall recommended another expression for spherical geometry at the Reynolds numbers range of $0 < \mathrm{Re} < 200$, in the form of [30]:

$$Nu_{d,sph} = 2.0 + 0.6\,\mathrm{Re}_d^{1/2}\,\mathrm{Pr}^{1/3} \tag{3.4}$$

Many different Nusselt number correlations have been introduced for the cylinders. The Collis and Williams correlation is frequently used for flow over cylindrical geometries for the Reynolds numbers in the range of 0.02 to 44 [29]:

$$Nu_{d,cyl} = 0.24 + 0.56\,\mathrm{Re}_d^{0.45} \tag{3.5}$$

Kramer's correlation is for a wider range of Reynolds number from 0.01 to 10,000 expressed as [22]:

$$Nu_{d,cyl} = 0.42\,\mathrm{Pr}^{0.2} + 0.57\,\mathrm{Pr}^{1/3}\,\mathrm{Re}_d^{1/2} \tag{3.6}$$

The difference in the value of Nusselt number obtained from the spherical and cylindrical correlations are evident just by comparing them at Reynolds number close to zero. At this condition Nusselt number equals 2.0 for a sphere, while $Nu \sim 0.3$ for a cylindrical geometry. Figure 3.2 shows how the selection of the Nusselt number correlation will result in different values.

As mentioned earlier, the choice of Nusselt number correlation is conventionally based on the geometry of the bead being spherical or cylindrical or a qualitative evaluation of the diameter of the thermocouple bead relative to the diameter of the thermocouple wire. Since the diameter of the bead is usually 1.5 – 3

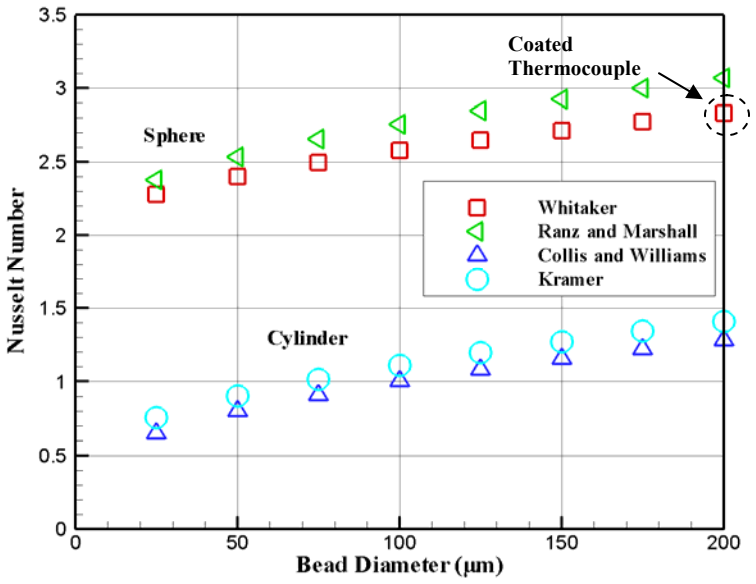

Fig 3.2: Calculated Nusselt numbers at a 900 K near flame location (Methane flame of ϕ = 0.65 and $\kappa_{mean} / \kappa_{ext} = 0.8$)

times the diameter of the wire, the spherical correlations are conventionally used for the thermocouples. The microscopic pictures of the thermocouples used in this study clearly showed the spherical geometry of the bead and also its diameter being at least two times the diameter of the wire. Therefore Whitaker correlation (eq. 3.3) was used to derive the Nusselt number as marked on figure 3.2.

Correct estimation of the properties of the gas surrounding a thermocouple is also an important factor in accurate calculation of gas temperature from the thermocouple measurements. Local gas properties such as viscosity, thermal conductivity, density, and the specific heat are required for calculation of the Nusselt number and convective heat transfer coefficient. Since evaluation of local gas properties is a strenuous task, properties of air or nitrogen at the local gas temperature are often used to approximate the gas properties [22]. In this study the properties of air at local temperature and the computational model velocities at each thermocouple position along with heat transfer correlations were used to calculate the Nusselt number, *Nu,* and the convective heat transfer coefficient, *h*.

3.2.2 Conduction

The conduction of heat between the thermocouple junction and the lead wire and support can be an important source of error in the temperatures measured by the thermocouple. The amount of conduction heat loss through the thermocouple wire is directly proportional to the longitudinal temperature gradients in the wire [22,31], and is expressed by Fourier's law:

$$\dot{Q}_{cond} = k_w A_w \frac{\Delta T}{\Delta x} \tag{3.7}$$

in which, $\dot{Q}_{cond}$ is the conduction heat transfer rate, k_w is the thermal conductivity of the thermocouple wire, A_w is the area through which heat is being conducted and $\Delta T/\Delta x$ is the temperature gradient through the length of the thermocouple wire. This gradient could be can be a result of temperature gradients in the gas. To reduce the conduction errors in the presence of such gradients, the thermocouple is aligned in a way that the length of the wire is along an isotherm.

The amount of conduction heat loss also depends on the length of the wire between the junction and support. To illustrate the conduction error corresponding to a given length of thermocouple wire, an energy balance is performed on the thermocouple wire. The analysis is simplified by assuming convection and conduction as the only sources of heat transfer around the thermocouple. Considering one-dimensional conditions in the longitudinal direction, monotonic temperature distribution, and uniform diameter, D, the temperature distribution along the thermocouple wire can be derived as [30]:

$$T(x) = (T_{supp} - T_g)\frac{\cosh\, m(L-x)}{\cosh\, mL} + T_g \tag{3.8}$$

where x is the distance from the support, $T(x)$ is the wire temperature at position x, T_{supp} is the support (lead wire) temperature, T_g is the gas temperature, and m is defined as $m = \sqrt{4h/kD}$. h is the convection heat transfer coefficient and L is half length of the exposed wire. The assumption of uniform diameter is only made to simplify the analysis since the bead is normally spherical and its diameter is 1.5 – 3 times the diameter of the wire. From this equation, the temperature at half length (at the junction) of the exposed wire, and the conduction error defined as T_g - $T(x)$ can be calculated. Figures 3.3 and 3.4 illustrate how the magnitude of conduction error varies with the length of a 50 μm thermocouple wire. Figure 3.3 shows the conduction cooling error defined when T_g - $T(x) > 0$ and figure 3.4 shows the conduction heating error when T_g - $T(x) < 0$.

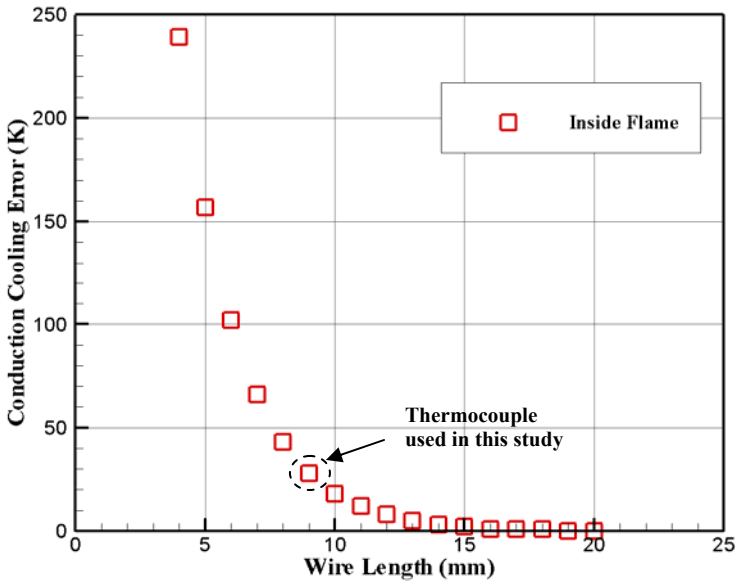

Fig. 3.3: Variation of conduction cooling error with thermocouple wire length in methane flame (ϕ = 0.65, α = 0.1 and $\kappa_{mean} / \kappa_{ext}$ = 0.6)

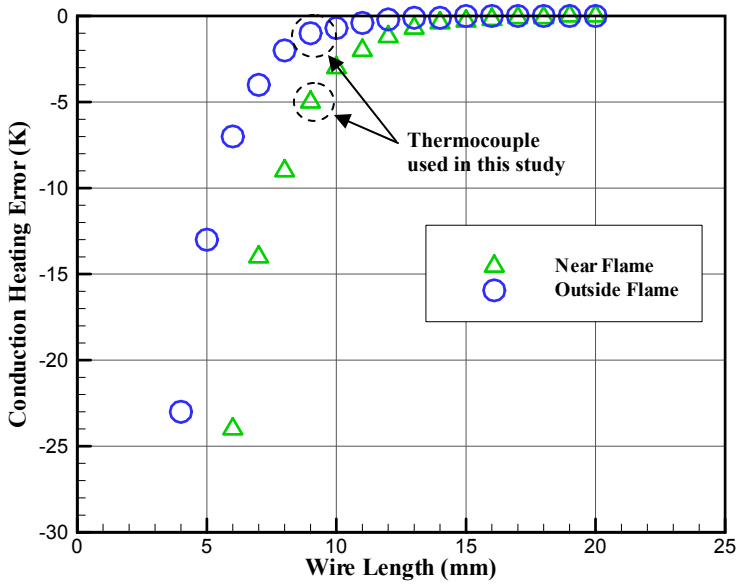

Fig. 3.4: Variation of conduction heating error with thermocouple wire length in methane flame (ϕ = 0.65, α = 0.1 and κ_{mean} / κ_{ext} = 0.6)

The thermocouple support is typically cooler than the thermocouple wire and junction as a result of more radiation loss to the surrounding [22], which may cause considerable conduction heat loss from the thermocouple wire and junction to the cooler support. Figure 3.3 illustrates this situation when the thermocouple is at a position inside the counterflow flame. As is evident in this figure, the conduction cooling error is more significant if the wire has a smaller length. Using longer lengths of thermocouple wire can reduce the conduction losses. In special cases, such as when the thermocouple support is closer to the flame than the thermocouple wire, for example the positions where the thermocouple wire is outside and parallel to the counterflow flame, the support will be closer to the flame because of its larger size and will conduct heat to thermocouple junction (Figure 3.5). Here also the amount of conduction error depends on the wire length (Figure 3.4).

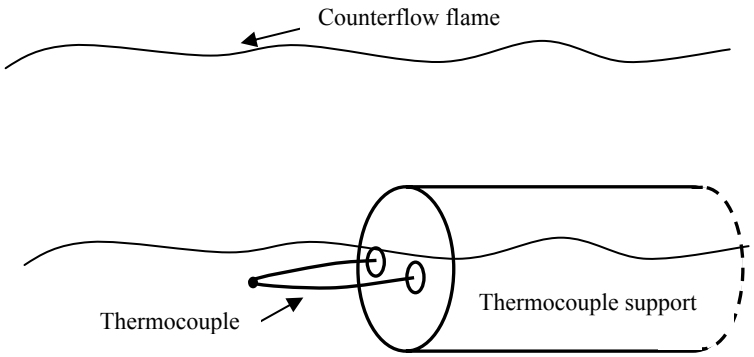

Fig. 3.5: Temperature difference between thermocouple and support

The values used for T_{supp} in these figures were from the support temperature measurements, which as mentioned in § 2.3.1 were over-predicting the difference between the exposed wire and insulated wire temperatures. Even with over-prediction of the conduction error, the magnitude of the error is insignificant for the 9 mm wire length used in this study.

In high velocity field it is more desirable to use short lengths of thermocouple wires to have a robust probe. However, according to Bradley and Mathews [32], if the length to diameter ratio, l/d_w, of the wire is below a minimum value such as 200, the conduction heat loss can be significant. Petit et al. [33], suggested that a better criterion was to use wires of length l such that $l/l_c > 10$, in which l_c is the characteristic length defined as $l_c = \sqrt{k_w d_w / 4h_{conv}}$. This criterion accounts for both the characteristics of the flow and of the sensor.

Values obtained from applying Petit criterion to the thermocouples used in this study with the exposed wire of 9 mm length and wire diameter of 50 μm at different locations in flame and out of flame, are in the range of 17 - 21 for the l/l_c

ratio which is above the recommended value of 10. Overall, the conduction error is considered negligible in this study.

3.2.3 Radiation

In general, the temperature of a thermocouple is affected by radiative heat exchange between its outer surface and the surroundings. The amount of this heat transfer is given by [30]:

$$\dot{Q}_{rad} = \varepsilon A \sigma (T_b^4 - T_{surr}^4) \tag{3.9}$$

where σ is the Stefan-Boltzmann constant $(\sigma = 5.67 \times 10^{-8}\ \mathrm{W/m^2 \cdot K^4})$, ε is the emissivity of the thermocouple surface, A is the surface area of the junction, T_b is the junction temperature, and T_{surr} is the surrounding surfaces temperature. This is a simplified analysis assuming the effect of radiation from other sources negligible and also constant value for T_{surr}.

Radiation losses are the most significant cause of error in the thermocouple temperature data especially at temperatures above 1000 K [34]. Assuming negligible conduction losses and catalytic effects by using sufficiently long thermocouple wires and applying non-catalytic coating on the thermocouple wire and junction, if required, energy balance of eq. 3.1 on the thermocouple junction can be expressed as:

$$\dot{Q}_{conv} + \dot{Q}_{rad} = 0 \tag{3.10}$$

which may be rewritten as:

$$T_g = T_b + \frac{\varepsilon \sigma}{h}(T_b^4 - T_{surr}^4) \tag{3.11}$$

Performing radiation corrections on the thermocouple measurements is not an easy task. Emissivity of the thermocouple, choice of Nusselt number correlations, the local gas properties, the size of the thermocouple, and thermal radiation sources surrounding the thermocouple are some of the factors that could change the amount of the radiation correction.

Emissivity, which is a radiative property of the thermocouple surface, strongly depends on the surface characteristics, i.e. material and finish, which may change by exposure to combustion environment [30]. Moreover, emissivity varies with temperature and wavelength [35]. For instance it has been found that in the temperature range of 600-900°C, emissivity of Pt-10%Rh wire can change as much as 40% [31]. Unfortunately, limited experimental data on emissivity of common thermocouple wires and non-catalytic coatings is available in literature.

An infrared camera was utilized to measure the emissivity of coated type R thermocouple. A thermocouple heating/cooling circuit that was originally designed for the time constant measurement (§ 3.6) is used for this measurement. During the heating cycle, DC heating current from a power supply flows into the thermocouple and heats it up. When the heating current is turned off, the peak temperature measured by the thermocouple just at the start of cooling cycle is recorded. Simultaneously, the infrared image of the thermocouple is taken and the peak temperature is determined. Since the emissivity value on the infrared camera system should be calibrated, in most cases the temperature from IR camera does not agree with the temperature from the thermocouple. This value should be adjusted on the IR system until the measurement function displays the same temperature as the

thermocouple. This adjusted emissivity is considered the emissivity of the thermocouple. The measurements were performed at low, medium, and high ranges of temperatures. Emissivity of the coated type R thermocouple in the temperature range of 600 – 1600 K varied in the range of 0.7 – 0.4.

The choice of the Nusselt number correlation will also affect the amount of radiation correction for the thermocouple measurements since the thermocouple radiation correction is inversely proportional to the convective heat transfer coefficient and Nusselt number($Nu = hd/k$). Figure 3.6 shows this effect when results from the correlations for spherical geometry are compared to cylindrical correlations.

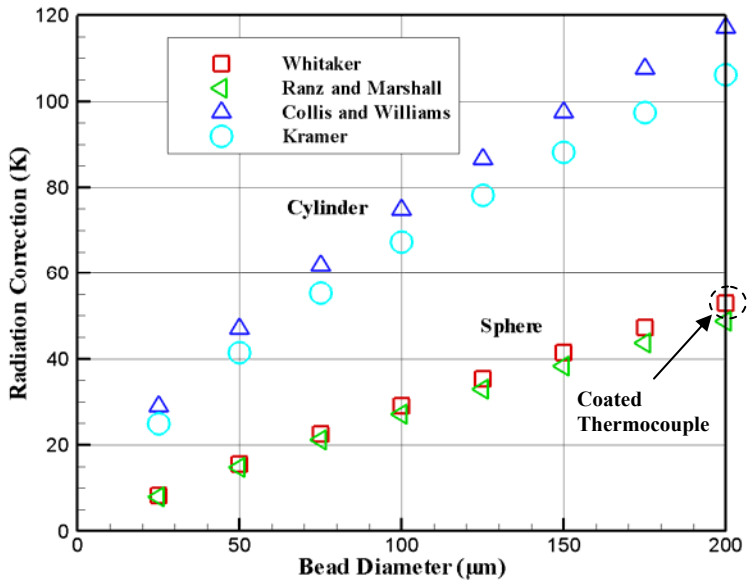

Fig. 3.6: Calculated radiation correction using Nusselt number correlations at a 900 K near flame location (Methane flame of ϕ = 0.65 and $\kappa_{mean} / \kappa_{ext}$ = 0.8)

As mentioned in § 3.2.1, a number of local gas properties are needed for calculation of Nusselt number and heat transfer coefficient. However, the local gas

properties are not usually known and may vary. In addition, there are some uncertainties in the Nusselt number correlations, which are based on experimental data [22].

Another important factor in the amount of radiation correction is the thermocouple size. The general recommendation for reducing the radiation losses is to use the smallest possible thermocouple junction and wire. Rewriting the equation 3.11, by utilizing definition of Nusselt number, shows the effect of thermocouple size:

$$T_g = T_b + \frac{d\varepsilon\sigma}{kNu}(T_b^4 - T_{surr}^4) \tag{3.12}$$

All Nusselt number equations correlate with $Re^{1/2}$, therefore with $d^{1/2}$. At low Reynolds numbers typical of the high temperature thermocouple measurements, the effect of Reynolds number on Nusselt number is considerably small. As a result, at these conditions the radiation corrections vary directly with thermocouple wire and bead size [22]. Figure 3.7 shows the effect of wire size on the amount of radiation errors at different thermocouple locations. Since radiation is proportional to T^4, it is clear that at high-temperature positions inside the flame a thermocouple bead will radiate more compared to low-temperature positions near or outside the flame. Moreover, the smaller convective heat transfer coefficient at locations inside the flame, contributes to larger radiation losses.

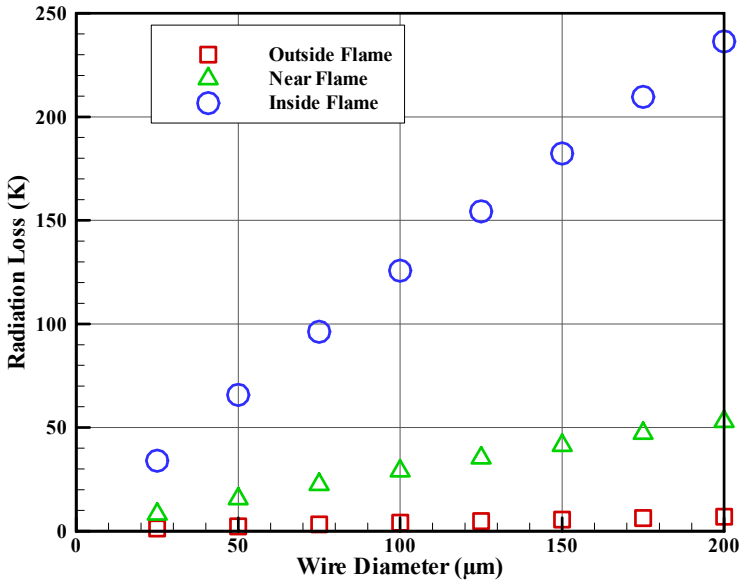

Fig. 3.7: Effect of thermocouple wire diameter on the radiation loss (Methane flame of ϕ = 0.65 and $\kappa_{mean} / \kappa_{ext} = 0.8$)

The thermal radiation sources surrounding a thermocouple such as the hot combustion gases and the flame may also affect the thermocouple measurement. This effect depends on the temperature, composition, concentration of emitting species, and path length [36]. In the absence of soot particles as in the non-luminous flames, CO_2 and H_2O are considered as the main emissive species in combustion products [37,38]. Using Hottel data on emissivities, Drysdale [36] illustrates that non-luminous flames have very low emissivities. Since the thickness of lean counterflow flames especially at close to extinction conditions is very small (~ 1mm), effect of radiation from hot gases on the thermocouple measurement is considered negligible.

3.2.4 Catalysis

In high-temperature combustion environments, platinum-based type R thermocouples are commonly used due to their high service temperature. Unoxidized fuel molecules and pyrolysis products in such environments, particularly those containing hydrogen use platinum as a catalyst for reaction and recombination. These recombination reactions can start at temperatures below 400°C [39]. At low temperatures, principally H_2 is participating in the reactions because its approximate lightoff temperature on platinum is between 100-150°C. Above 550°C, methane becomes active and thus CH_4 and any pyrolysis products can be oxidized on platinum [40]. If there is enough hydrogen in the gas flow to heat up to methane lightoff temperatures, even at low temperatures very high thermocouple temperatures can be read.

Once chemical reactions are initiated they produce heat, causing error by raising the temperatures measured by the thermocouple [22,26,31,34]. Catalytic activity is highest in the pre-flame zone and the reaction zone and depends on concentration of un-burned fuel, local mean temperature, time at that temperature, and on the hydrogen content of the fuel [31].

The best method for reducing or eliminating catalytic effect is to coat the thermocouple with a non-catalytic material, which must also be impermeable to flame gases. Three common types of coatings used are: silica-based coating, beryllium oxide/ yttrium oxide ceramic, and alumina-based ceramic. Silica-based coating can be applied as a thin coating with relatively low emissivity. However, it has been found to be very fragile [26] and to react with hydrogen at temperatures above

1100°C. The BeO/Y_2O_3 coating also forms a thin coating but is not very stable, has large emissivity, and is highly toxic. Alumina-based ceramic coatings have become more common in recent years because of their stability at high temperature. Yet, due to their viscous nature, they form a thicker coating.

Although coating reduces the catalytic effect, it increases the thermocouple diameter, the response time of the thermocouple, and the radiation losses. It also changes the convective and conductive heat transfer of the thermocouple. Therefore, in order to get the best results a very thin layer of coating should be applied. Since the coating changes the heat transfer properties of the thermocouple, it is difficult to quantify the effect of catalysis. However, a qualitative comparison of type R measurements with type K thermocouple measurements, at positions where the temperatures were below the melting point of type K thermocouple, showed satisfactory reduction in the catalytic effects after coating the thermocouple.

3.3 Non-uniform Thermocouple Heating

Another source of error in the thermocouple measurements is the non-uniformity of temperature distribution within the thermocouple junction and wires. This non-uniformity will reduce the sensitivity of the thermocouple [41] or cause conduction errors.

Physical and thermal properties of the thermocouple itself may be the reason for such non-uniform heating. The Biot number, defined by $Bi = hL/k$, where L is characteristic length, h is convective heat transfer coefficient, and k is the thermal conductivity of the wire, provides a measure of rate of convective heat transfer to the

thermocouple bead and wires relative to radial thermal conduction within the thermocouple [22]. If $Bi << 1$, the temperature drop in the thermocouple junction relative to the temperature difference between the thermocouple surface and the surrounding gas will be very small and at this condition it is reasonable to assume uniform temperature distribution across the thermocouple [30].

As mentioned in § 3.2.2, in the presence of temperature gradients in the combustion gas, the thermocouple should be aligned along an isotherm to minimize the conduction errors. Yet in some flame configurations the temperature gradients are so large that can produce internal temperature gradients even in small diameter thermocouples with $Bi << 1$. For instance, the temperature gradient across the thermocouple bead in the counterflow methane flame of the present study ($\varphi = 0.65$, $U_{inj} = 7$ m/s, $\kappa/\kappa_{ext} = 80\%$) could be as large as 600 K. According to Weckmann [41] at this condition the temperature measured by the thermocouple is either assumed to be the highest temperature at the junction or an average temperature of the junction.

3.4 Thermocouple Positioning

Since temperature measurements are tied to a position, an important issue with the thermocouple measurements is the errors introduced by movement or vibration of the thermocouple. These movements can be generated from flaws in the support or the positioning system, or can be a result of alternating thermal expansion and contraction of the thermocouple wire as it moves from one temperature region to another, especially at regions with high temperature gradients [34]. Utilizing a robust

support and positioning system and minimizing the length of the fine thermocouple wire (§ 2.2.2 and 2.3.1) were measures taken to reduce the errors in this study.

3.5 Probe-induced Disturbances

Thermocouple intrusion in the gas stream may cause the measured temperatures to be different from what is characteristic of undisturbed stream. According to Fristrom [34], the aerodynamic effect of thermocouple intrusion on the flame will produce a velocity-deficient wake that deforms the flame and displaces the isothermal surfaces in the flow that are flat otherwise (Figure 3.8). This deformation moves the flame closer to the thermocouple. As a result, the thermocouple tends to record higher temperatures than what is characteristic of that position in an undisturbed flow. Minimizing the size of the thermocouple can reduce this error.

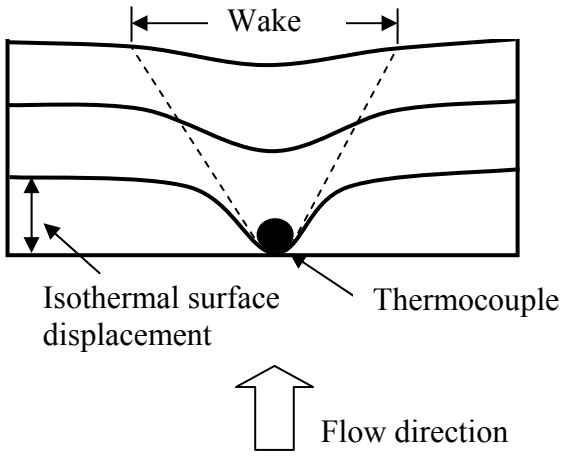

Fig. 3.8: Probe-induced disturbances [34]

3.6 Thermal Inertia

When measuring high-frequency temperature fluctuations, thermal inertia of the thermocouple will cause a delay in the response of the probe to the input heat flux. Thus, the thermocouple output will be attenuated and phase-delayed. This temporal lag is characterized by the thermocouple time constant and should be compensated to recover the fluctuations of gas temperature from the measured data [27,31,32].

The time constant of the thermocouple is defined as the time the probe takes to respond to the changes in its surrounding temperature. Assuming conduction losses from the thermocouple as well as catalytic reactions on the probe surface to be negligible, the energy balance of the equation 3.1 on the thermocouple bead can be rewritten as:

$$\dot{Q}_{conv} + \dot{Q}_{rad} + \dot{Q}_{stor} = 0 \tag{3.13}$$

or [27],

$$T_g(t) = T_b(t) + \tau \frac{dT_b(t)}{dt} + \gamma(T_b^4(t) - T_{surr}^4) \tag{3.14}$$

where τ is the characteristic response time or time constant of the thermocouple, and γ is the ratio of radiative effects to convective effects as shown by:

$$\tau = \frac{m_b c_p}{hA_b} \tag{3.15}$$

$$\gamma = \frac{\varepsilon\sigma}{h} \tag{3.16}$$

Equation 3.15 shows that the time constant of the thermocouple is not only related to the physical properties of the thermocouple, i.e. the mass of the

thermocouple junction, m_b, the specific heat, c_p, and the surface area of the junction, A_b, but also depends on heat transfer coefficient of the flow, h. Determining the value of c_p and h is difficult since they are dependent on local temperature, velocity, and composition of the flow [31]. Moreover, changes in the geometrical shape of the bead after coating introduces more uncertainties in determining the exact surface area, A_b, of the bead.

A more conventional method to directly determine the time constant is to use the temperature step change method [27]. In this method τ is found from the response time of the thermocouple to a step change in the temperature of the probe. For a thermocouple system where radiation losses are negligible, τ can be defined as the time taken for the thermocouple temperature to decay to 1/e of this step change as shown in figure 3.9 because the governing equation is first order with respect to temperature. In this method a DC electrical current heats the thermocouple junction

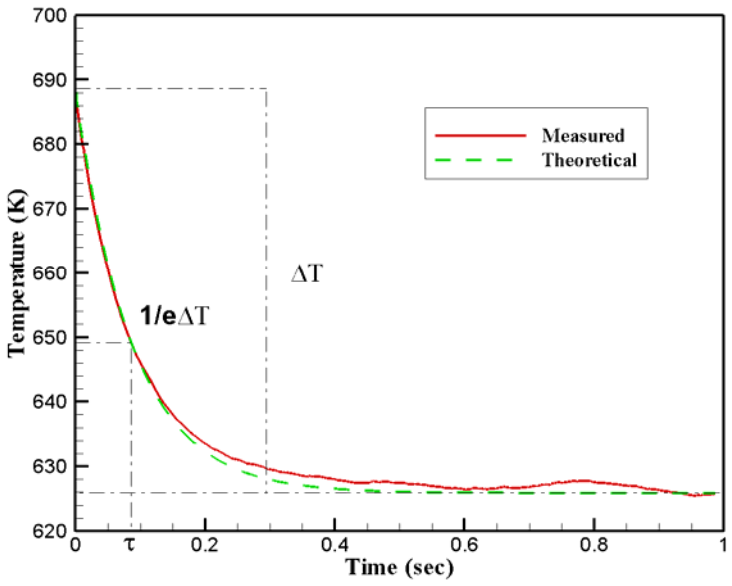

Fig. 3.9: Average temperature decay for calculation of the time constant

above the local flame temperature. The over-heat temperatures are kept relatively small $50\text{K} < \Delta T < 100\text{K}$ so it does not significantly affect the local flame characteristics. The heating current is then switched off to create a step change from the overheat temperature to the local flame temperature. The thermocouple temperature subsequently decays to this local flame temperature. The heating and cooling cycles are repeated hundreds of times and the average time constant is found from ensemble averaging of the decay cycles. An average decay curve from 100 heating/cooling cycles is shown in figure 3.9. The theoretical exponential decay curve corresponding to the measured time constant is also displayed. As the figure shows, average decay curve is in reasonable agreement with the theoretical exponential decay, which validates the first-order assumption of the system.

Average local time constant is measured using a switching circuit designed to trigger the heating/cooling cycles at the appropriate times. The set-up for the measurement is shown in figure 3.10. Two fast response solid-state relays with maximum on/off time of 50 μs are employed to isolate the heating and cooling cycles. During the heating cycle, a TTL signal from the DAQ computer to the heating circuit relay closes the circuit and DC heating current from a power supply flows into the thermocouple. When the heating current is turned off, another TTL signal triggers the cooling circuit relay and thermocouple voltage decay is collected by the amplifier and the data acquisition board. The number of heating cooling cycles, the time period for each cycle, and the frequency of thermocouple data collection are controlled by a LabVIEW program developed for this purpose. An IDL program is also developed to average the decay cycles and calculate the time constant for each set of

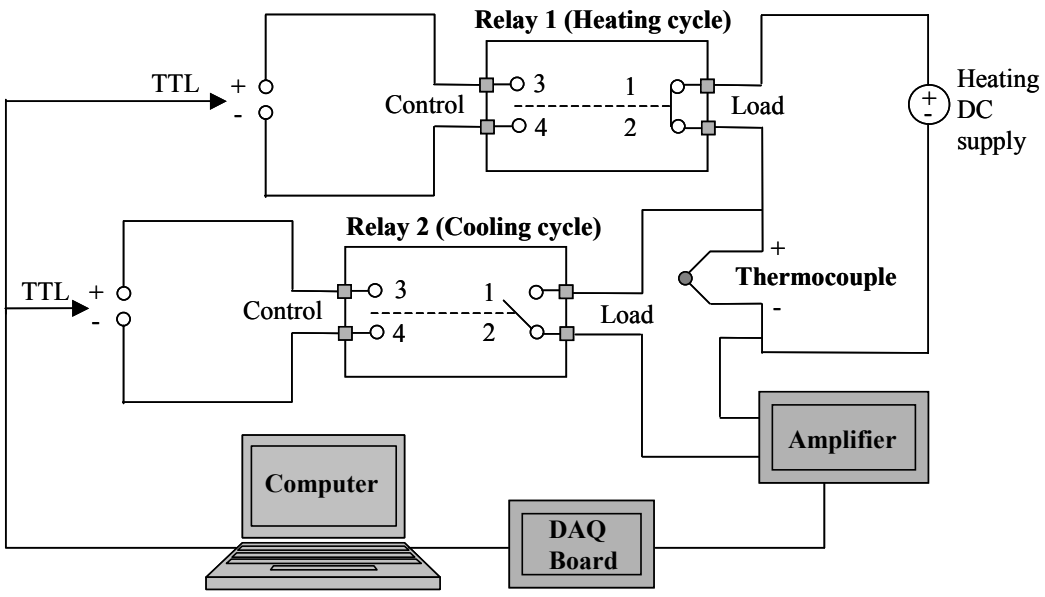

Fig. 3.10: Experimental set-up for measuring response time of the probe

measurements. Temperature step change of the average decay curve is calculated from the initial temperature as the maximum and the average of the last 1/10 of the data points as the stable minimum temperature of the decay curve. For the coated type R thermocouple in the temperature range of 1070 K < T < 1770 K time constants in the range of 100 ms < τ < 320 ms were obtained. The measured τ was unrealistically large. Ultimately, the velocities from the analytical model [5], were used along with the heat transfer correlations to determine the convective heat transfer coefficient, *h* at each measurement location to obtain the time constant.

With the knowledge of average time constant value, the thermal inertia of the thermocouple can be compensated. However, compensation of thermal inertia based on equation 3.14 involves calculation of time derivative of temperature, which may be inaccurate when dealing with discrete values. In order to avoid errors in the calculation of the derivative, differentiation of the transient term is performed in the

frequency domain using Fourier transform [27]. Thus, the gas temperature can be expressed as:

$$T_g(t) = T_b(t) + \mathrm{FFT}^{-1}\left[j\tau\omega T_b(\omega)\right] + \gamma(T_b^4(t) - T_{surr}^4) \tag{3.17}$$

where $T_b(\omega)$, is the Fourier-transformed temperature (calculated with Fast Fourier Transform), ω is the frequency, and FFT^{-1} is the inverse Fast Fourier Transform. A program written in IDL [27] is used to digitally compensate for thermal inertia and radiation effects at the thermocouple junction. Assuming negligible radiation effect, the compensation program was applied on a simple sinusoidal temperature signal to show the difference between uncompensated and compensated signals. As illustrated in figures 3.11 and 3.12, uncompensated signal is attenuated and phase-delayed compared to compensated signal. The attenuation and phase difference depends on the frequency of temperature oscillations and the time constant of the thermocouple. Figure 3.11 demonstrates how for a certain value of time constant, larger frequency of temperature fluctuations will results in larger error in uncompensated data. Also comparison of figures 3.11 (a) and 3.12 (a) or figures 3.11 (b) and 3.12 (b) shows how larger time constant will result in larger attenuation and phase delay. It may be concluded that compensation process compensates for amplitude and phase delay in raw data.

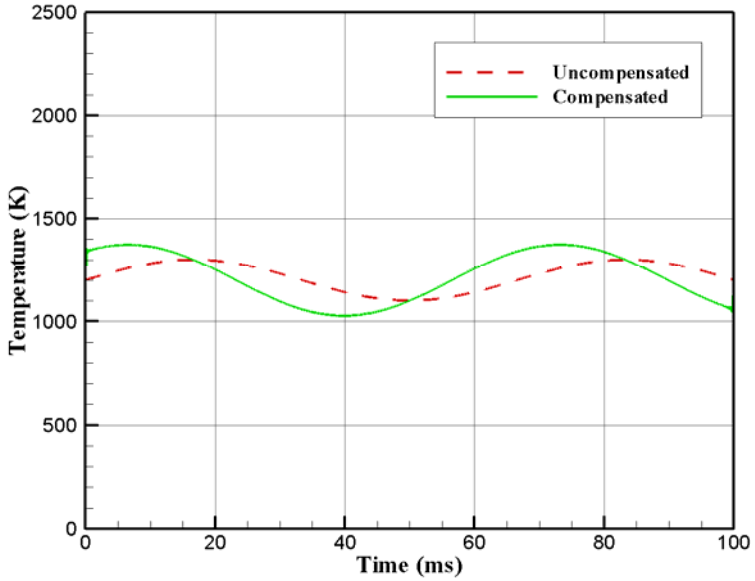

(a) Frequency = 15 Hz

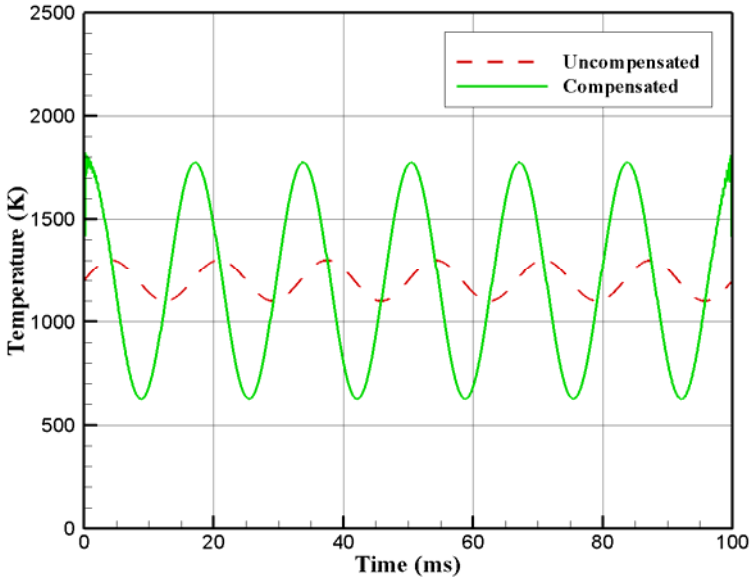

(b) Frequency = 60 Hz

Fig. 3.11: 100 ms of uncompensated and compensated sinusoidal signal at τ = 15 ms

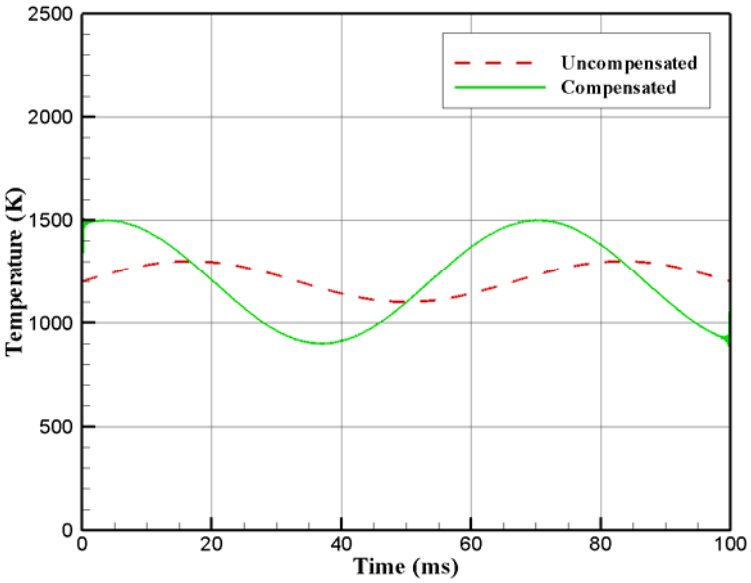

(a) Frequency = 15 Hz

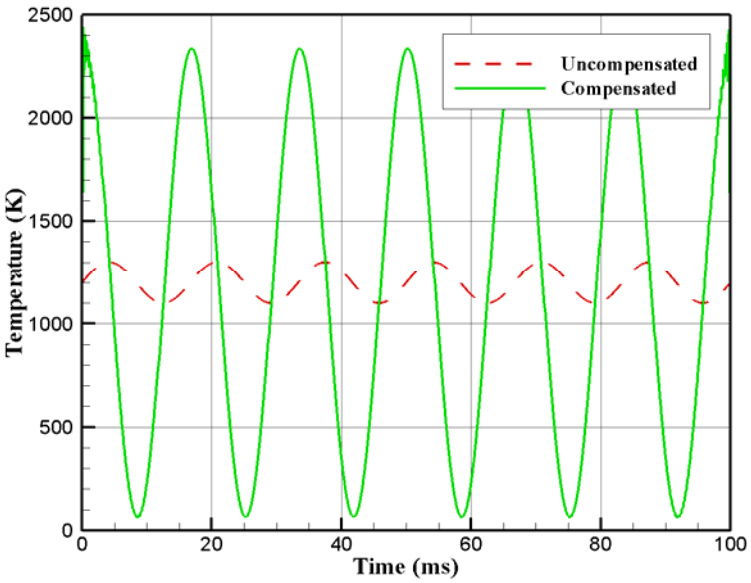

(b) Frequency = 60 Hz

Fig. 3.12: 100 ms of uncompensated and compensated sinusoidal signal at τ = 30 ms

3.7 Measurement Validation

The thermocouple data were not compared directly with other experimental results since no data with similar experimental conditions to our experiments were found. Instead, our data were compared with a FORTRAN-based computational code adapted from CHEMKIN-based premixed code that was shown to predict the flame behavior accurately [17,25]. The model is used to calculate the flow velocity, temperature, and species mass along the central axis of the nozzles within a cylindrically symmetric counterflow premixed flame. The model can predict the behavior of methane flame with and without hydrogen doping as a function of strain rate.

In this section, first it is established that the computational results can accurately simulate the thermal behavior of the strained flame at the conditions used by another independent experimental study. Next, there is a discussion on how the uncertainty in parameters such as equivalence ratio or strain rate will cause uncertainty in the choice of comparable computational data.

3.7.1 Model Quality Assessment

The experimental condition of an independent study by Law et al. [21] was simulated and the computed temperature profile was compared to the experimental data from that study. The experiments were conducted in a counterflow configuration with nozzle diameter of 14 mm at separation distance of 11 mm. The near-stoichiometric ($\phi = 0.95$) methane/air mixture of Law's study was diluted by nitrogen to achieve extinction strain rates which were within the capability of the flow system.

The temperature measurements were derived from the shape of Raman spectrum. A comparison between experimental and computed temperature profile at one of the experimental conditions in Law's investigation is illustrated in figure 3.13. Although the measurements were performed at much lower strain rates (< 400 s^{-1}) compared to strain rates of the present study in the range of 2500 $s^{-1} < \kappa_{mean} < 6700\ s^{-1}$ and at larger nozzle separation compared to the present study, the computed results are found to have reasonable agreement with the experimental data, hence supporting the validity of the computational model for the simulation of strained flames.

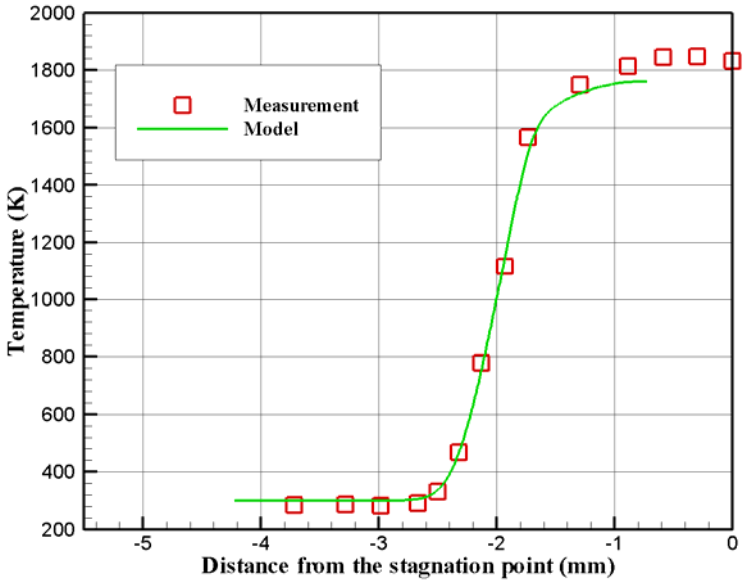

Fig. 3.13: Comparison between computed profiles and Raman scattering temperature profiles (Case C, $\kappa_{mean} / \kappa_{ext} = 0.5$, $\kappa_{ext} = 400\ s^{-1}$) [21]

3.7.2 Uncertainty in Experimental Parameters

As mentioned earlier, the experiments of this study have been conducted at a specific equivalence ratio and strain rate. However, there are some uncertainties in the experimental value of these parameters which can be due to instrumentation e.g.,

from the mass flow controller, the heaters, leakage of un-burned fuel or from facility and environmental effects. According to Sai [25], 8% uncertainty in the strain rate and 3% uncertainty in the equivalence ratio are estimated for the experiments of this study. These experimental parameters are used as input in the computational model to simulate the behavior of the flame. Therefore, our measurement data is compared to the computational model at both boundaries of these errors. Figure 3.14 illustrates comparison of measurement and computational temperature profiles for pure methane ($\phi = 0.65$, $\kappa_{mean} / \kappa_{ext} = 0.8$). The measurement results are corrected for the radiation effect once with the assumption of spherical bead geometry and another time with the assumption of cylindrical bead geometry. The computational profile is calculated for both the low and high boundaries of temperature.

The uncertainty in the gas temperature due to measurement systematic errors, are calculated for each measurement location and the results are presented in figures 3.14 (a) and (b). Since coating the thermocouple introduces uncertainty in defining the geometry of the bead, the calculations are done for both spherical bead geometry (figure 3.14 (a)) and cylindrical bead geometry (figure 3.14 (b)). The figures clearly show that our basic assumption of spherical geometry is the more appropriate one.

These figures are intended to give an idea of the errors involved in the measurement. However, errors due to thermocouple positioning, probe induced disturbances in flame and temperature gradient across the thermocouple bead are not considered in the calculations because of the difficulty in quantifying them. Figure 3.14 is a representative of the magnitude of errors that could be present in this study

and should be kept in mind while reviewing the results in the next chapter. More details can be found in Appendix B.

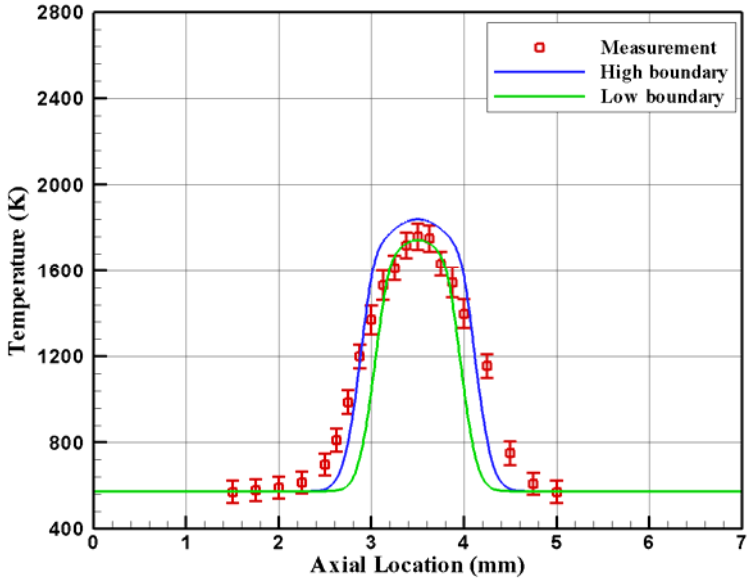

(a)

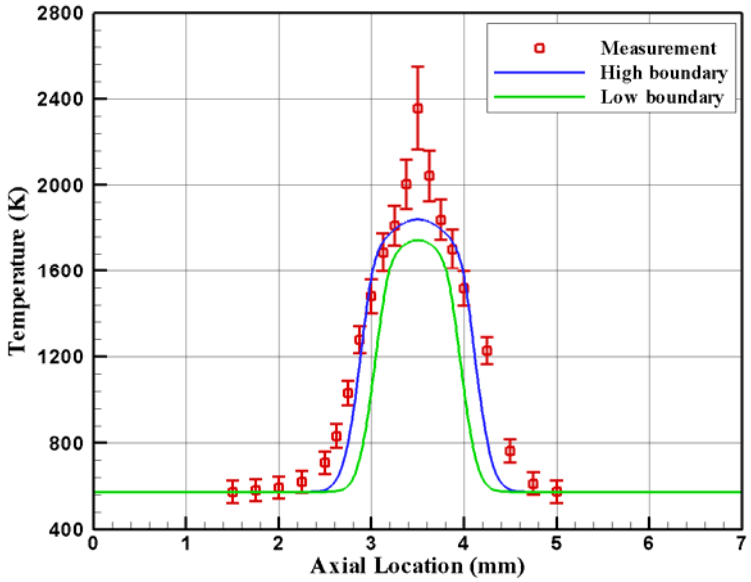

(b)

Fig. 3.14: Uncertainty in experimental conditions **(a)** Spherical bead geometry **(b)** Cylindrical bead geometry

Chapter 4: Results

4.1 Introduction

As mentioned earlier in § 2.4, the hydrogen doped mixtures are characterized by equivalence ratio, ϕ, defined as the fraction of O_2 consumed by both fuel components combined and by α, the fraction of O_2 consumed by H_2. In the current study the mixture ϕ was kept constant at 0.65 and α ranged from 0.0 to 0.1 and the flow was preheated to 300 °C. In this chapter the temperature measurement results for steady and forced flame and the effect of strain and hydrogen doping on the thermal characteristics of methane flames will be evaluated. The measurement results are corrected for radiation losses with the assumption of spherical bead geometry and in the case of oscillating flames compensated for thermal inertia.

4.2 Steady Flames

4.2.1 Effects of Strain

Figure 4.1 shows the profiles of centerline axial temperatures of the counterflow flame measured by the thermocouple. The origin of the axial location is assumed to be at the upper nozzle. The lower nozzle is located at 7 mm and the stagnation plane is located at 3.5 mm. The α ranged from 0.0 to 0.1 and the strain rate varied at $\kappa_{mean} / \kappa_{ext} = 0.6$ and $\kappa_{mean} / \kappa_{ext} = 0.85$ corresponding to far from and close to extinction conditions, respectively. Experiments showed that increasing H_2 content in the fuel decreased the sensitivity of the flame to positive strain and higher strain rates were needed to reach close to extinction conditions (Table 4.1).

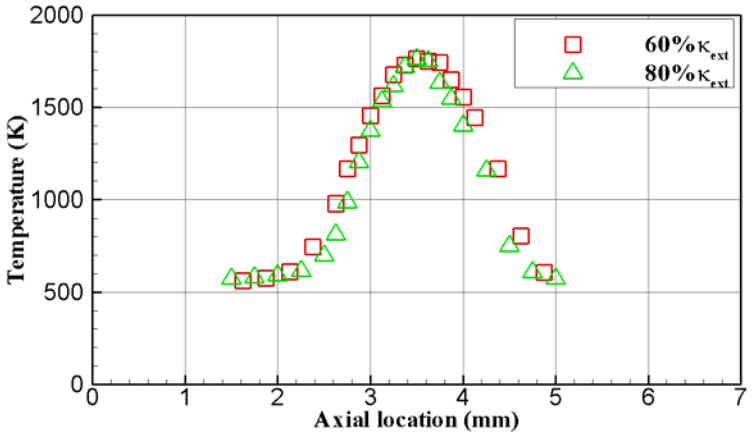

(a)

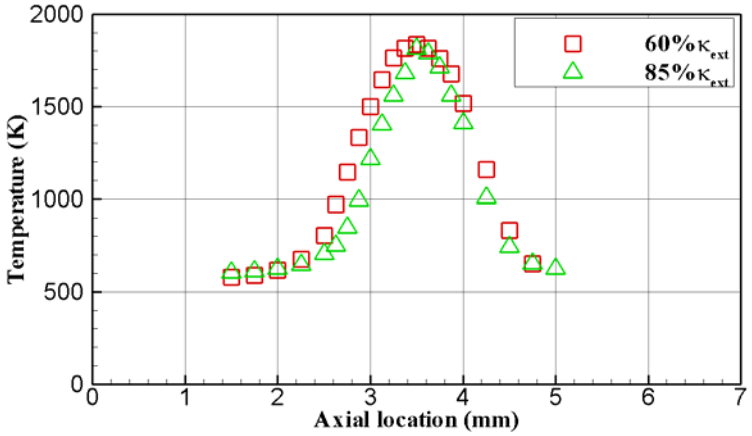

(b)

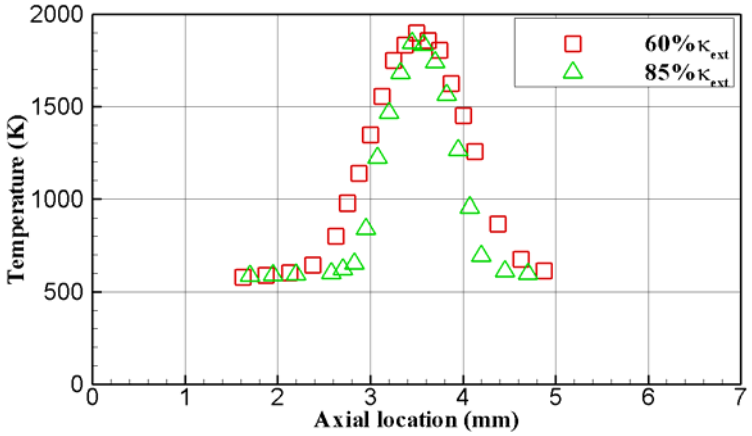

(c)

Fig. 4.1: Effect of strain on CH_4 flames – Measurement result (ϕ = 0.65)
(a) α = 0.00 **(b)** α = 0.05 **(c)** α = 0.10

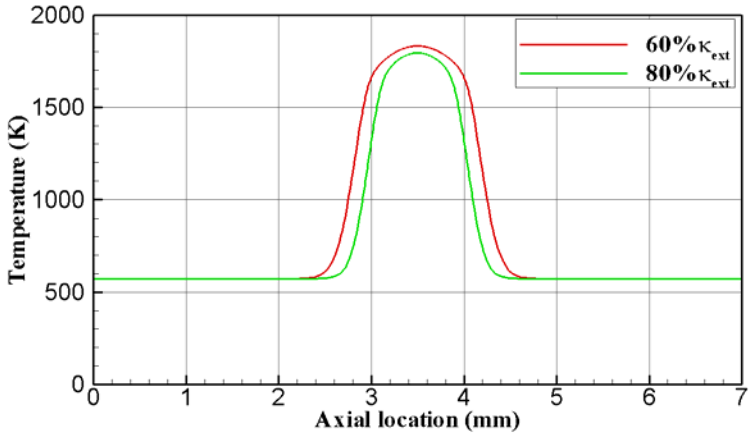

(a)

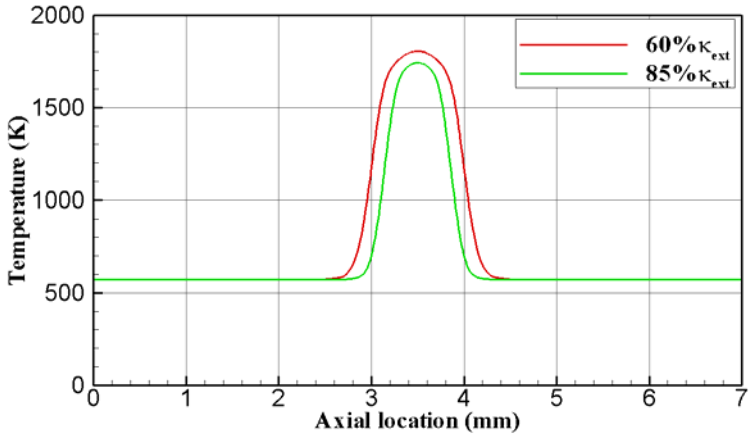

(b)

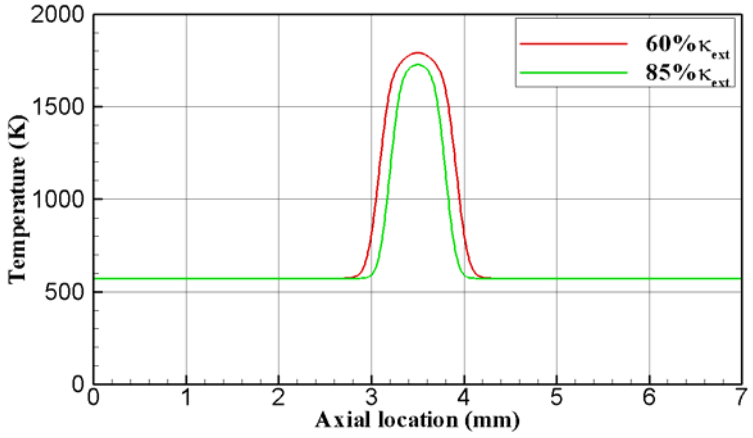

(c)

Fig. 4.2: Effect of strain on CH_4 flames – Modeling results (ϕ = 0.65)
(a) α = 0.00 **(b)** α = 0.05 **(c)** α = 0.10

In general it is predicted (figure 4.2) that for the high strain rate conditions of this study, the flame temperature decreases with increasing the strain rate [25]. Table 4.1 presents the measured flame temperature at the stagnation plane. Although model predicts larger differences in the flame temperatures (40-60K) for the flames at the same conditions, the measurement results especially at $\alpha = 0.10$ (figure 4.1.c) show the same trend of decrease in flame temperature with increase in strain rate.

Comparison of the width of the flames as indicated in table 4.2, shows that as the strain rate increases the flame thickness decreases. The calculated width of the flame in this study was based on the distance above and below the maximum temperature where the gas temperature was greater than 75% of the temperature rise [20]. Similar calculations for the model predictions presents the same trend but 10 to 25% smaller widths as the α changes from 0.00 to 0.10, respectively.

Finally, maximum temperature gradients increase as the strain rate increases for each fuel mixture (Table 4.2). However, the predicted temperature gradients do not change significantly when the strain rate is increased for pure methane or at conditions of α up to 0.10.

Table 4.1: Measured and adiabatic CH_4 flame temperature

ϕ	α	$\kappa_{mean} / \kappa_{ext}$ (%)	κ_{mean} (1/s)	T_{adiab} (K)	T_f (K)
0.65	0.00	60	1500	1973	1763
		80	2000		1758
0.65	0.05	60	2714	1984	1835
		85	3857		1813
0.65	0.10	60	4043	1994	1898
		85	5714		1833

Table 4.2: Flame width and temperature gradient

ϕ	α	κ_{mean} / κ_{ext} (%)	κ_{mean} (1/s)	Flame width (mm)	Gradient (K/mm)
0.65	0.00	60	1500	1.2	1350
		80	2000	1.0	1500
0.65	0.05	60	2714	1.0	1400
		85	3857	0.7	1450
0.65	0.10	60	4043	0.8	1700
		85	5714	0.6	2750

In general, the measurement results follow the predictions of the effect of strain on the flame structure but there are some quantitative differences such as higher recorded temperatures especially at positions away from the flame. These differences could be attributed to the effect of thermocouple intrusion on the flame which results in recording higher temperature downstream of its physical position or could be the result of exothermic catalytic reactions.

4.2.2 Effects of Fuel

When hydrogen is added to the fuel, the doped flame resists higher values of strain rate. As a result, higher strain rates are needed to reach close to extinction conditions (Table 4.1). These higher strain rates will reduce the flame width. This effect is shown in Figure 4.3. This figure illustrates the comparison of experimental temperature profiles of methane mixtures with α varying from 0.00 to 0.10 at conditions far from extinction (a), and close to extinction (b). Figure 4.4 presents the model profiles. The same trend is observed for the width of the flames.

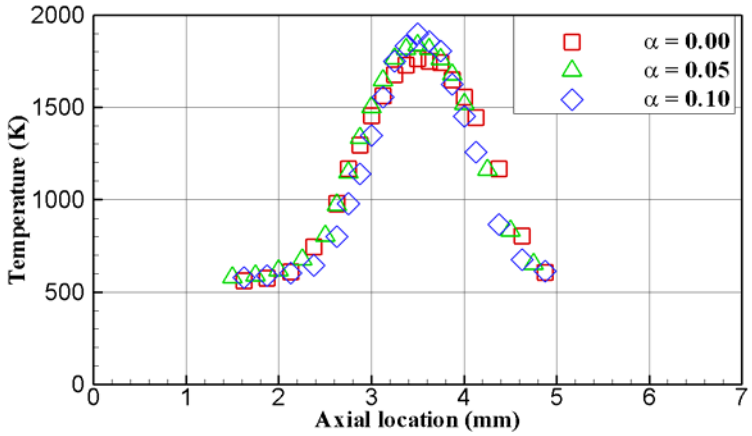

(a)

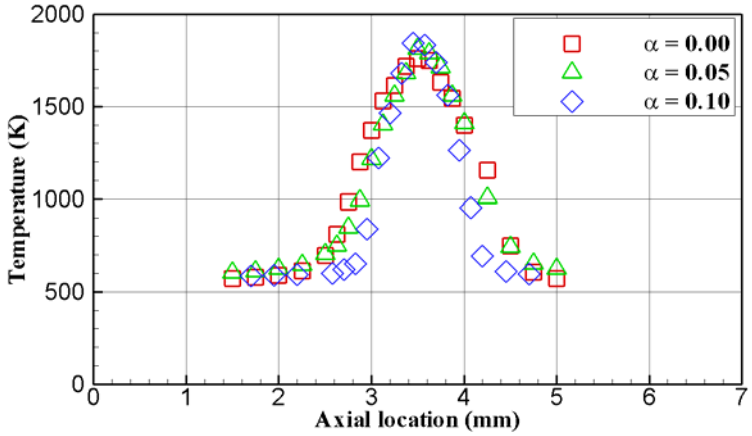

(b)

Fig. 4.3: Effect of H_2 addition on CH_4 flames – Measurement results (ϕ = 0.65) **(a)** 60% of κ_{ext} **(b)** CH_4 at 80% and CH_4/H_2 at 85% of κ_{ext}

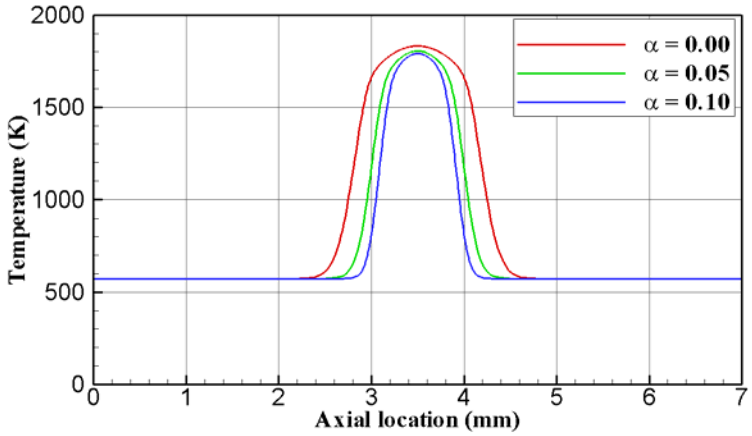

(a)

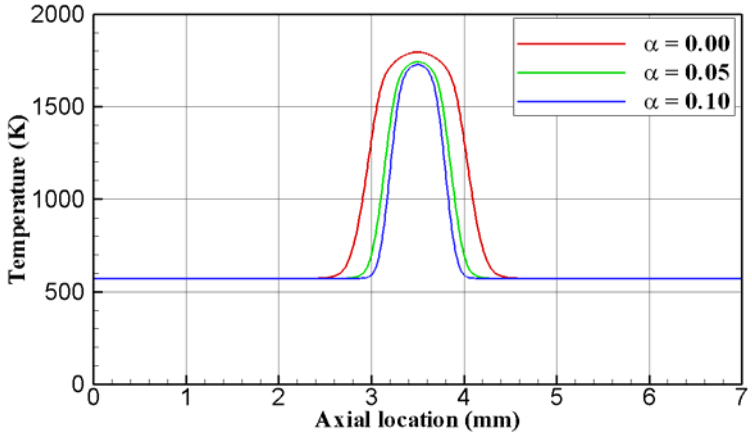

(b)

Fig. 4.4: Effect of H_2 addition on CH_4 flames – Modeling results (ϕ = 0.65) **(a)** 60% of κ_{ext} **(b)** CH_4 at 80% and CH_4/H_2 at 85% of κ_{ext}

Comparison of the adiabatic temperatures of methane flame with α varying from 0.00 to 0.10 shows a small increase in the flame temperature (Table 4.1). Sai [25] shows that for a constant ϕ and κ, the predicted flame temperature increases as α is increased but at close to extinction conditions the flame temperature does not change significantly with the addition of H_2 (Figure 4.5).

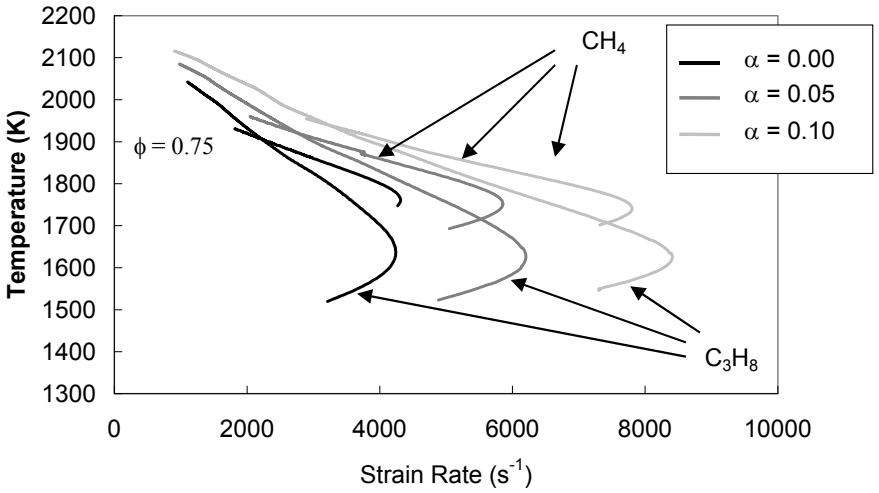

Fig. 4.5: Changes in the flame temperature as a function of strain rate for CH_4 and C_3H_8. Extinction occurs at tip of the knee of the profiles [25]

No significant difference in the peak temperatures is observed in figures 4.3.and 4.4. However the methane flame is predicted to have a slightly higher peak flame temperature than the hydrogen doped mixtures. This is to be expected, since the comparisons are made at the same percentage of κ_{ext}, and the absolute value of κ_{mean} for pure methane is less than those for $\alpha = 0.05$ or $\alpha = 0.10$. The effect of thermocouple intrusion on the flame could be the reason for the discrepancy in the trend of change in the peak temperatures.

3.3 Oscillating Flames

A preliminary investigation on the effects of oscillation on near extinction flames was done in the earlier stages of this study. At the time a ceramic ZrO_2 coating was carefully brushed onto the exposed surfaces of the probe to prevent catalytic effects which increased the measurement junction diameter to 150 μm. This coating was later replaced with the Aremco Ceramabond coating which gave more

satisfactory results. The velocities from the analytical model were used along with the heat transfer correlation to determine the convective heat transfer coefficient, h at each measurement location to obtain the time constant τ. The forced velocity oscillations in this investigation result in a time-varying τ. However, changes in τ owing to these fluctuations are negligible, typically less than 2%. A relative narrow range of average time constants, 24 ms < τ < 32 ms, were determined. To reduce the effective response time of the probe, a compensation technique, discussed in the previous chapter was used. Figure 4.6 illustrates a sample temperature signature in the flame brush of a weakly strained methane flame having $\phi = 0.65$ and a forcing amplitude of $u'/u_{mean} = 0.15$. The measured data is also corrected for the radiation losses.

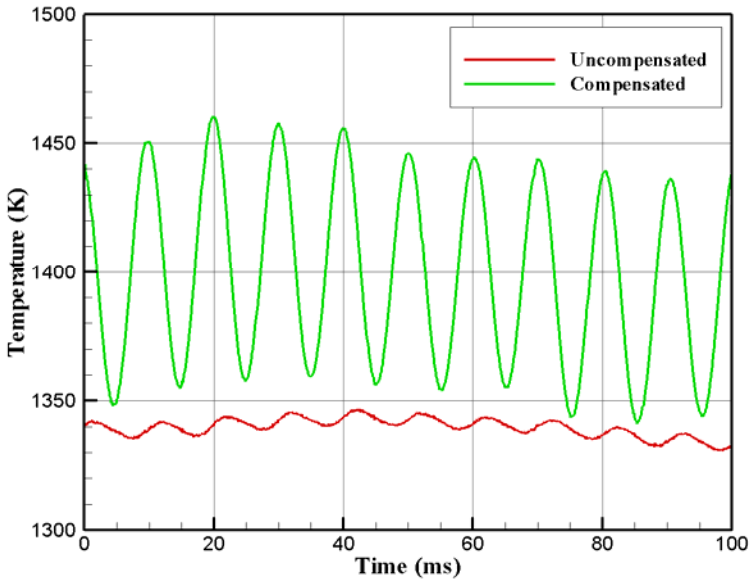

Fig. 4.6: Uncompensated and compensated temperature signatures in the methane flame brush ($\phi = 0.65$, $\alpha = 0.0$, $u'/u_{mean} = 0.15$)

Temperature measurements under steady and oscillating conditions were performed in H_2-doped ($\alpha = 0.10$) flames near extinction having $\phi = 0.65$, and $\kappa_{mean} / \kappa_{ext} = 0.9$. Mean and fluctuating (standard deviation) flame temperature profiles for these cases are provided in figure 4.7. The figure shows that the measured peak

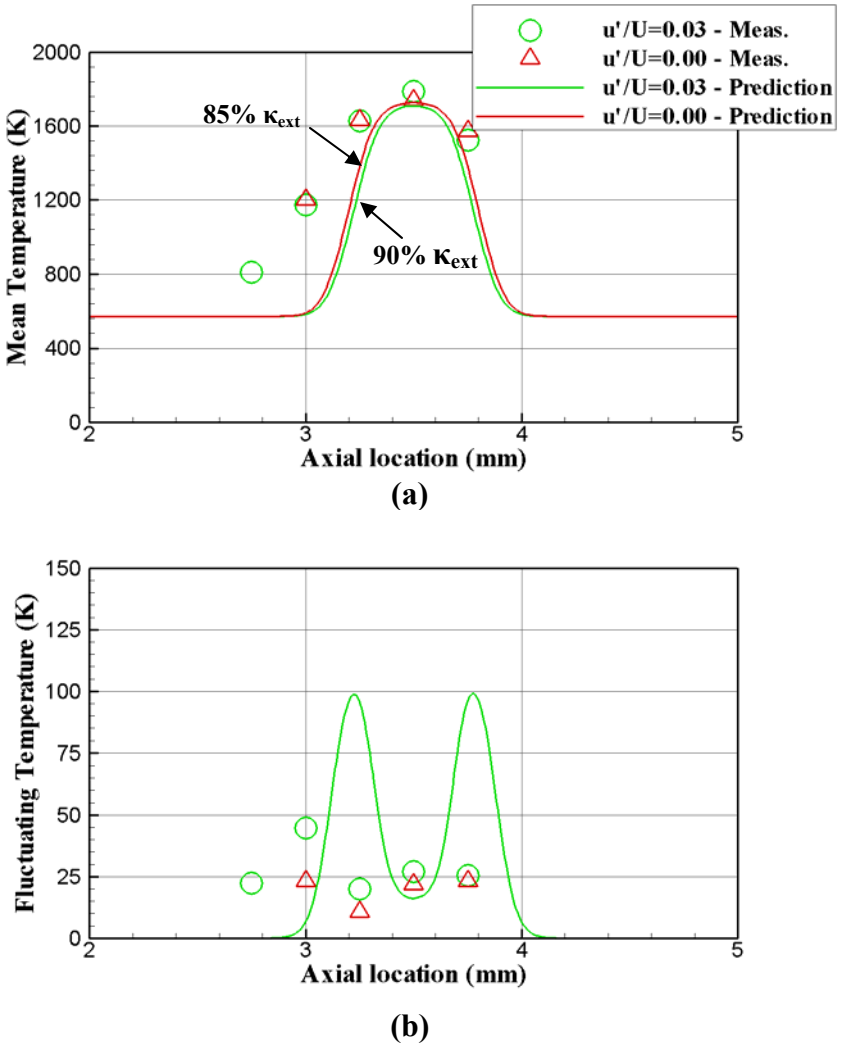

Fig. 4.7: Measured and calculated (a) mean and (b) fluctuating temperature profiles for $\phi = 0.65$, $\kappa_{mean} / \kappa_{ext} = 0.9$, $T_{in} = 300$ °C for (Δ - $\alpha = 0.10$, $u'/u_{mean} = 0.0$), ($\bigcirc$- $\alpha = 0.10$, $u'/u_{mean} = 0.03$).

centerline temperatures are in good agreement with the predicted peak temperature. The measurements and model predictions demonstrate the mean temperature at close to extinction conditions does not change considerably with the magnitude of the forcing amplitude for the small forcing amplitudes used in this study. However, modeling predictions and measurements show that changes in the forcing amplitude will impact the temperature fluctuations. Also in contrast to the modeling, the measurements show that standard deviations in temperature are present even in the steady case, most likely due to fluctuations in ϕ that persist into the flame.

Chapter 5: Conclusions

In this study, the effects of hydrogen addition on the thermal behavior of lean-premixed methane flames in highly strained counterflow fields were investigated. Temperature profiles were obtained using Pt/Pt-13% Rh micro-thermocouple. Since thermocouple produces disturbances in the flame structure, the effects of the probe are reduced by minimizing the size of the thermocouple. Measuring the temperature with the thermocouple in the CH_4/H_2 combustion environment and the thin counterflow flames of this study was found to be specially challenging. Since catalytic reactions in the reducing atmospheres especially those containing hydrogen and methane could produce large errors in thermocouple readings, special attention was paid to find a suitable coating and to apply a thin coating to minimize the catalytic effect errors. Quality of measurements was improved by changing the thermocouple support design to minimize the thermocouple movement and also by utilizing an automated micro-positioning system. The thermocouple wire was aligned in a way that the length of the wire was along an isotherm to minimize the conduction errors and the measurements were post-processed to correct for radiation losses. In the case of preliminary work on the oscillating flames, a compensation technique was used to reduce the response time of the thermocouple.

Experimental results were compared with numerical modeling results. At close to extinction conditions a slight reduction in flame temperature with increase in strain is observed. This could be due to the increase in the convective heat loss as the strain is increased. Increase in strain will also reduce the flame width by pushing the flame closer to the stagnation surface to keep the balance between the flame speed

and the flow velocity. Both near to and far from extinction H_2-doped mixtures, produce thinner flames in comparison with pure methane at the same $\kappa_{mean} / \kappa_{ext}$ because of the corresponding higher strain rates. Also no significant variation in peak temperatures is observed between different fuel types.

However, there are some discrepancies between the measured and predicted temperature values especially at positions away from the stagnation plane. These discrepancies could be a result of disturbances in the gas stream caused by the thermocouple intrusion which deforms the flame and moves the flame closer to the thermocouple, or could be produced by catalytic errors still present. Although the intrusion effect explains the broadening of the flame when measurements are done by thermocouple probes, it is not clear how to correct for this effect. Non-intrusive diagnostics are needed for further analysis in such thin flames.

Appendix A: Illustration of National Instruments LabVIEW Program Utilized for Temperature Measurement and Traverse Control

Program front panel:

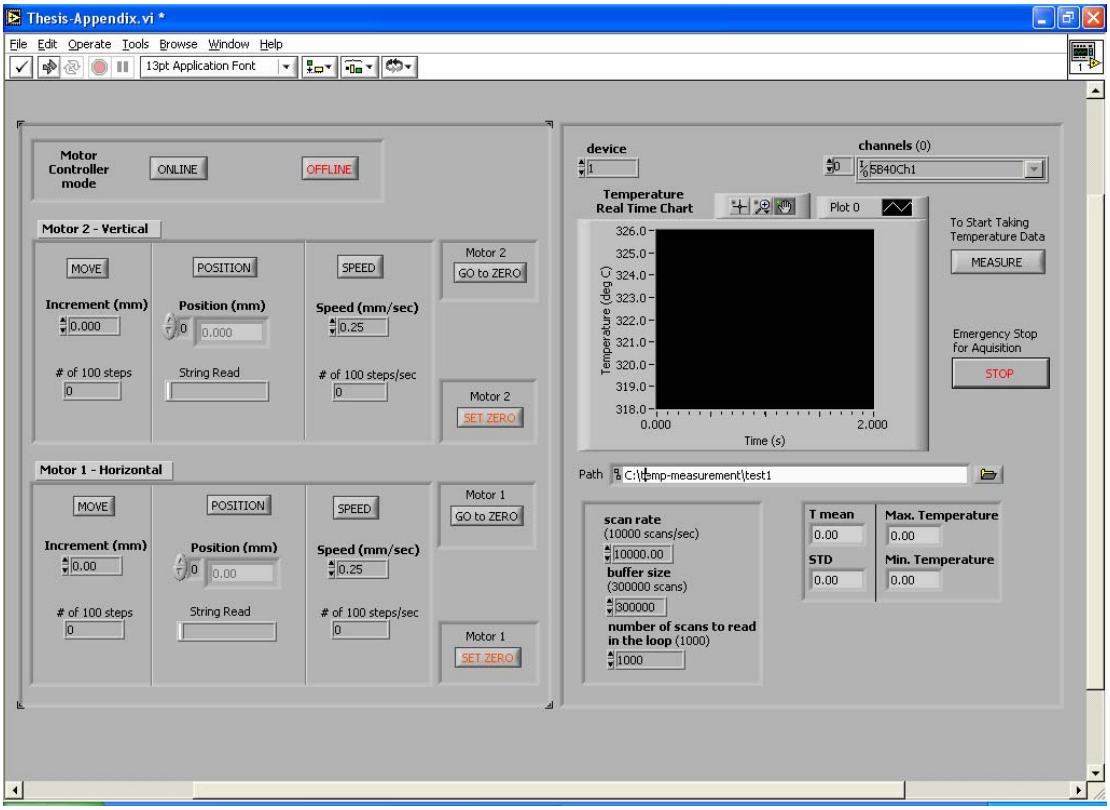

Diagram Window: (Shown in several sections)

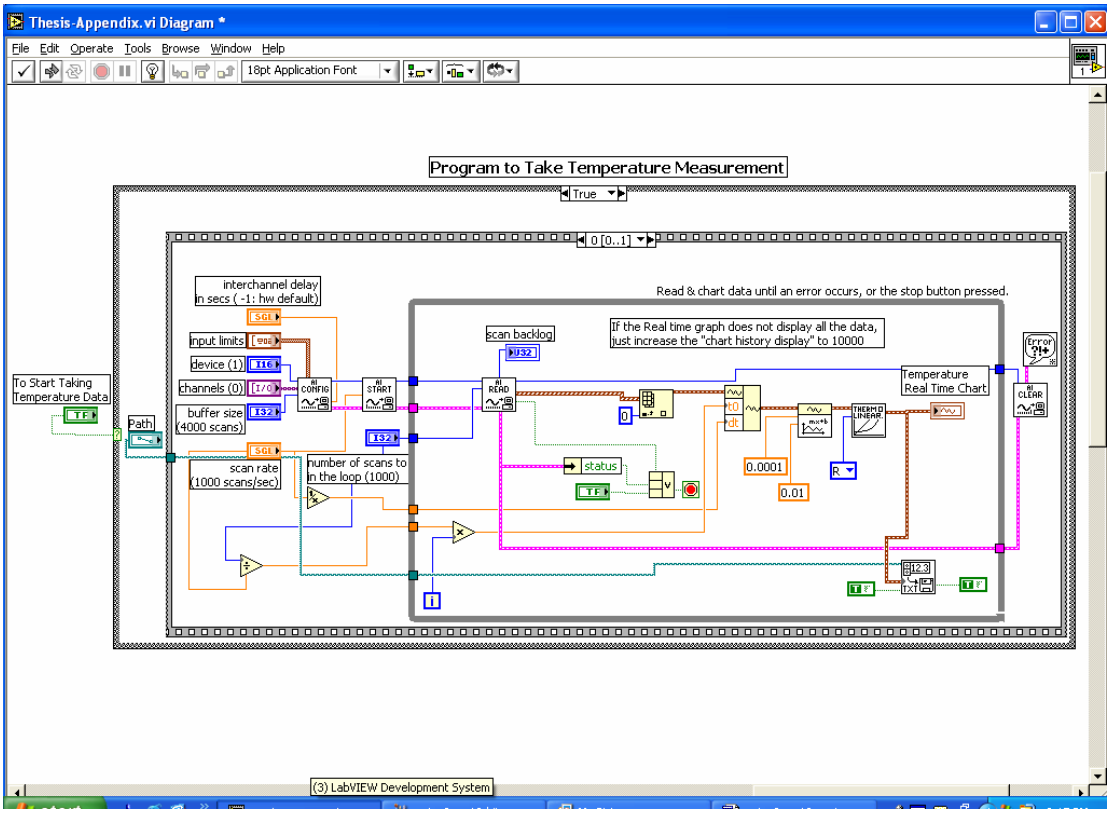

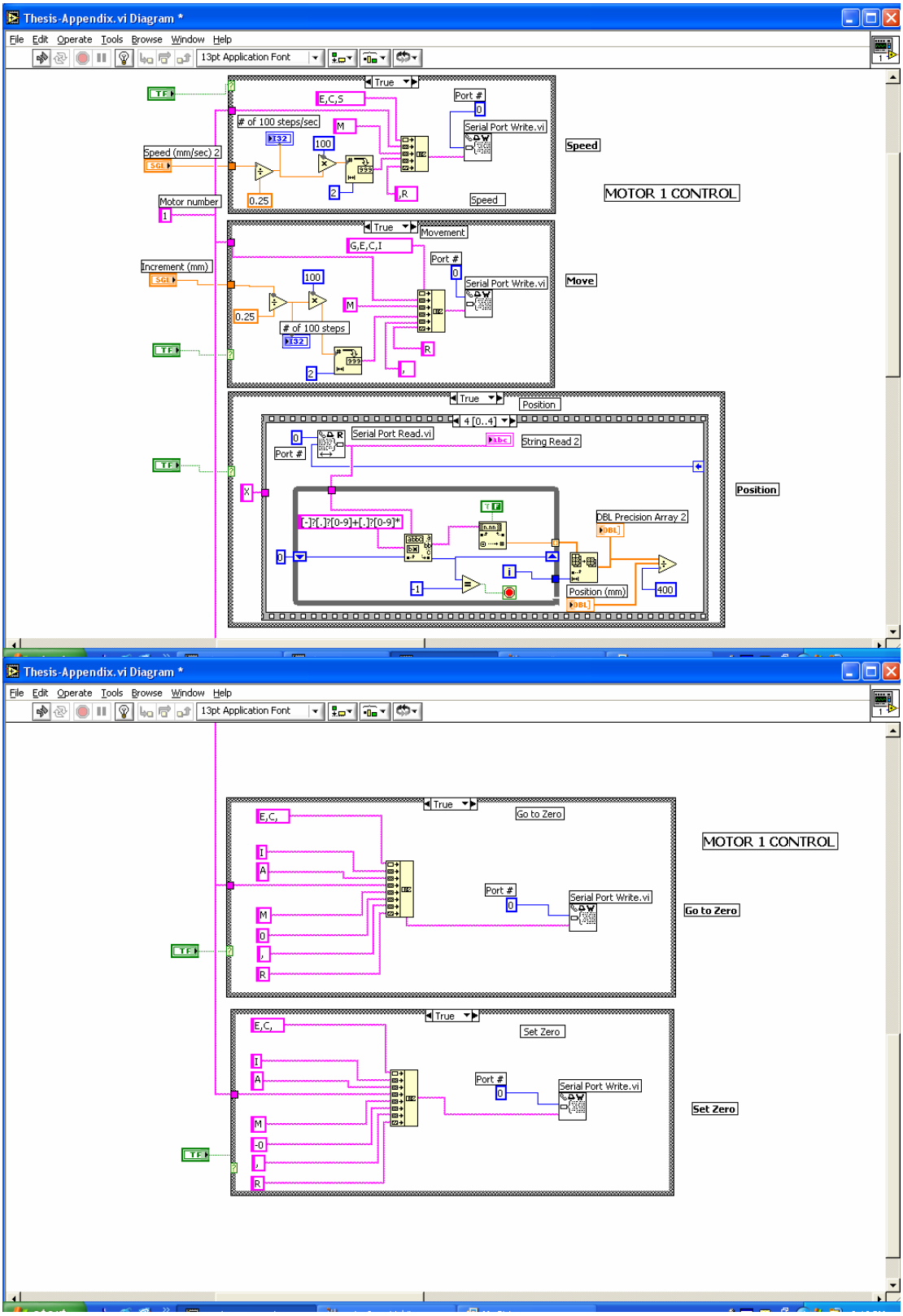
Thesis-Appendix.vi Diagram *
File Edit Operate Tools Browse Window Help
13pt Application Font
True
E,C,S
Port #
# of 100 steps/sec
M
Serial Port Write.vi
Speed (mm/sec) 2
100
Speed
0.25
2
,R
Motor number
MOTOR 1 CONTROL
Movement
G,E,C,I
Increment (mm)
Move
# of 100 steps
R
Position
Serial Port Read.vi
4 [0..4]
String Read 2
[-]?[.]?[0-9]+[.]?[0-9]*
DBL Precision Array 2
Position (mm)
400
-1
Thesis-Appendix.vi Diagram *
E,C,
Go to Zero
Set Zero
-0

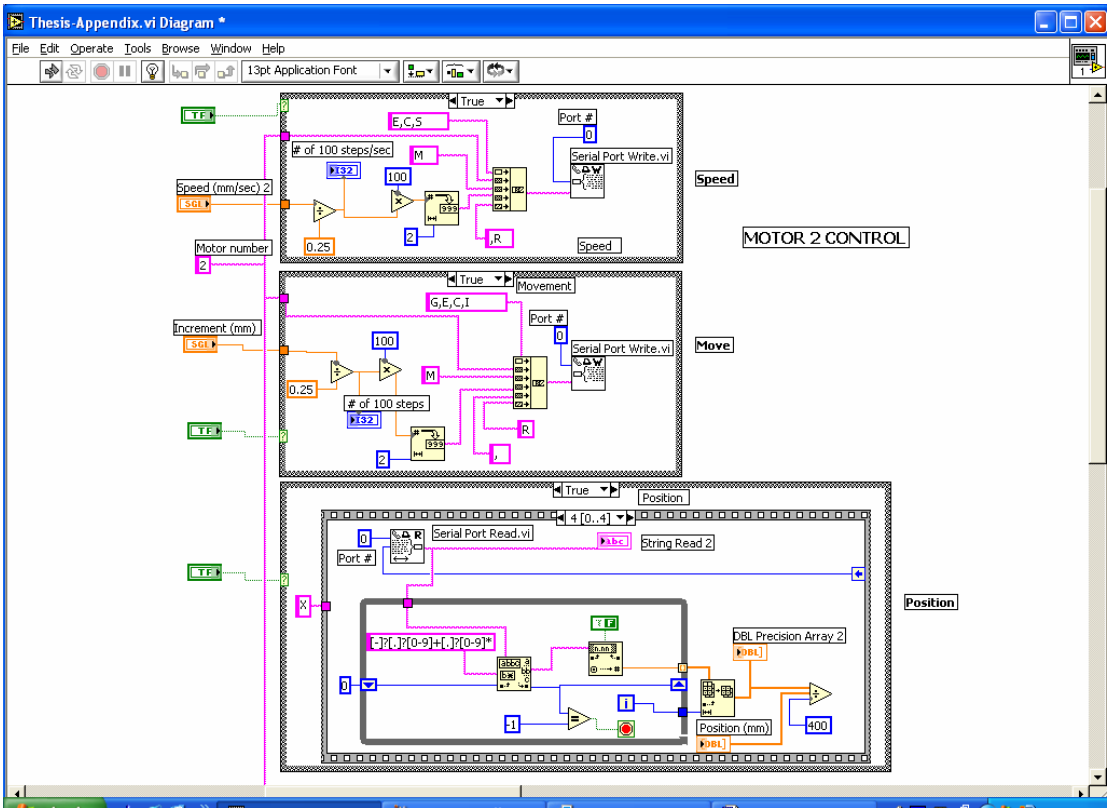
Thesis-Appendix.vi Diagram *
File Edit Operate Tools Browse Window Help
13pt Application Font
True
E,C,S
Port #
# of 100 steps/sec
M
Serial Port Write.vi
Speed (mm/sec) 2
100
Speed
Motor number
0.25
2
,R
Speed
MOTOR 2 CONTROL
True
Movement
G,E,C,I
Port #
Increment (mm)
100
Serial Port Write.vi
Move
0.25
M
# of 100 steps
R
2
True
Position
4 [0..4]
Serial Port Read.vi
String Read 2
Port #
[-]?[.]?[0-9]+[.]?[0-9]*
DBL Precision Array 2
Position
Position (mm)
400
-1

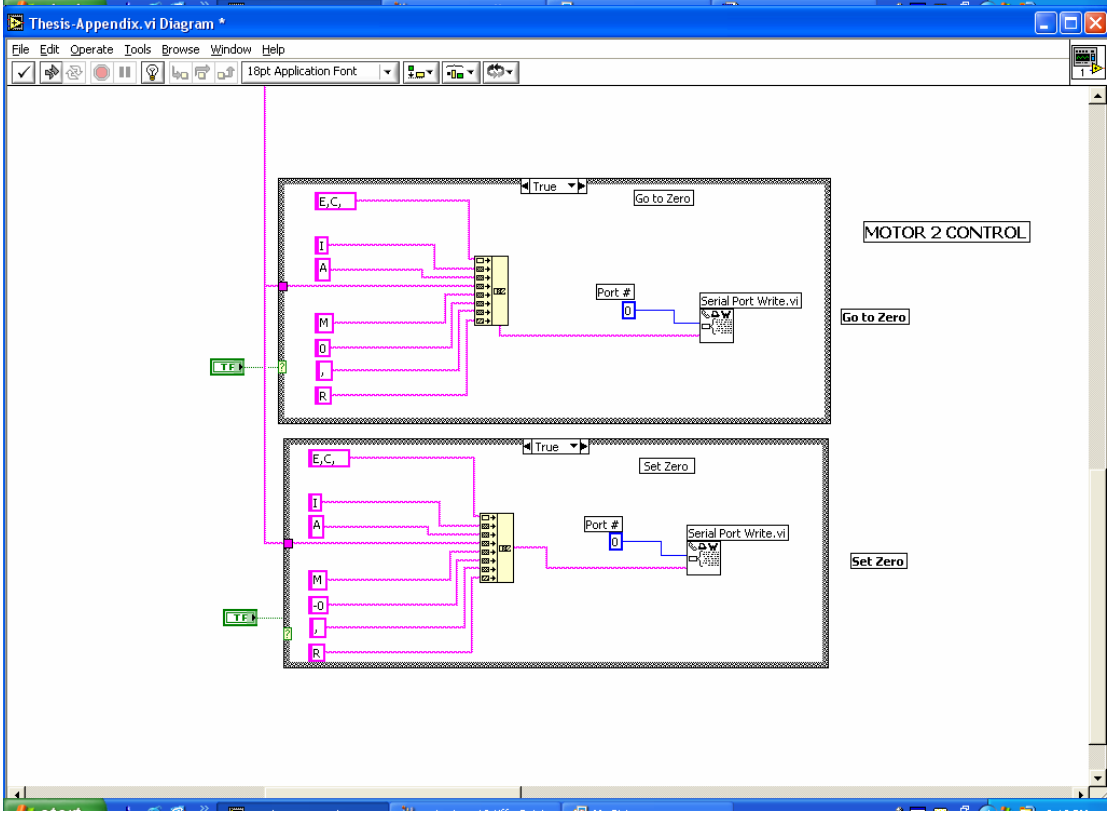
Thesis-Appendix.vi Diagram *
File Edit Operate Tools Browse Window Help
18pt Application Font
True
E,C,
Go to Zero
MOTOR 2 CONTROL
I
A
Port #
Serial Port Write.vi
M
0
,
R
Go to Zero
True
E,C,
Set Zero
I
A
Port #
Serial Port Write.vi
M
-0
,
R
Set Zero

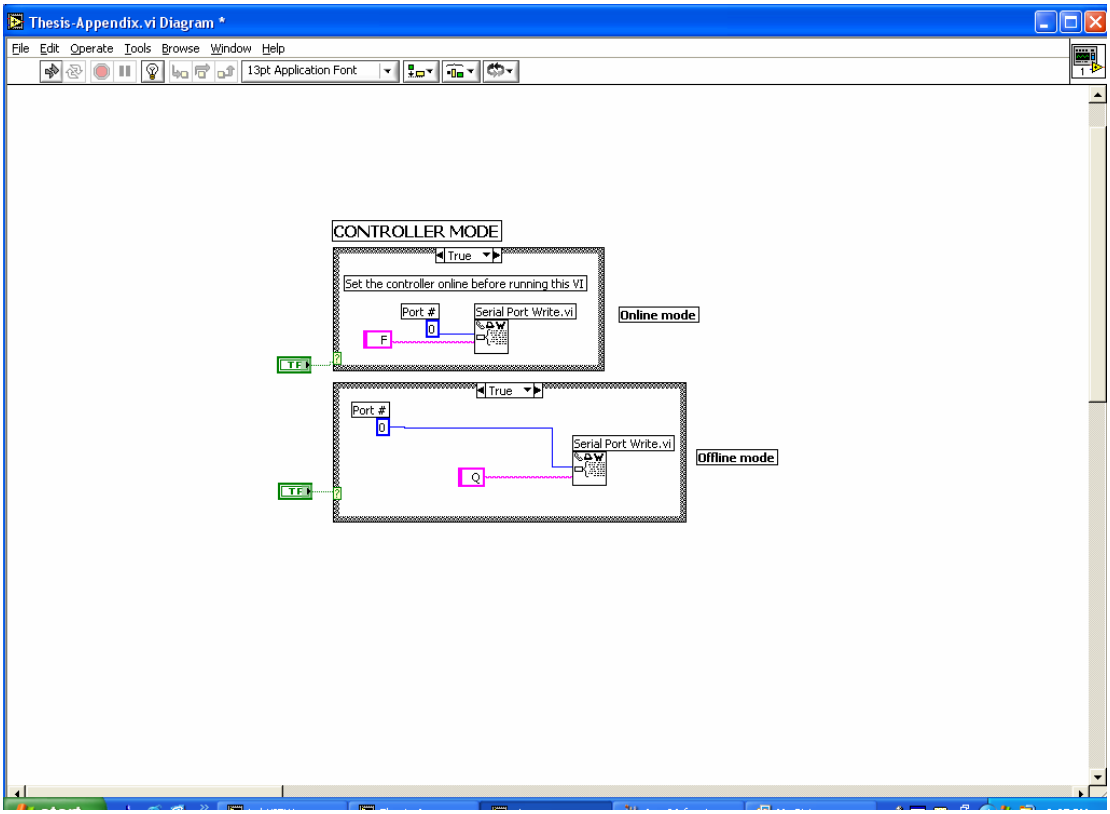
Thesis-Appendix.vi Diagram *
File Edit Operate Tools Browse Window Help
13pt Application Font
CONTROLLER MODE
True
Set the controller online before running this VI
Port #
0
Serial Port Write.vi
F
Online mode
TF
True
Port #
0
Serial Port Write.vi
Q
Offline mode
TF

Appendix B: Error Analysis for Steady-State Thermocouple Measurements

Energy balance on the thermocouple can be expressed as:

$$\dot{Q}_{conv} + \dot{Q}_{rad} + \dot{Q}_{cond} + \dot{Q}_{cat} + \dot{Q}_{stor} = 0$$

where $\dot{Q}$ is defined as net rate of heat outflow. In steady-state condition $\dot{Q}_{stor} = 0$,

$\dot{Q}_{conv} = h(T_b - T_g)A_s$, and $\dot{Q}_{rad} = \varepsilon\sigma(T_b^4 - T_{surr}^4)A_s$. Substitution results in:

$$h(T_b - T_g)A_s + \varepsilon\sigma(T_b^4 - T_{surr}^4)A_s + \dot{Q}_{cond} + \dot{Q}_{cat} = 0$$

Solving in terms of T_g gives:

$$T_g = T_b + \frac{\varepsilon\sigma}{h}(T_b^4 - T_{surr}^4) + \frac{\dot{Q}_{cond}}{hA_s} + \frac{\dot{Q}_{cat}}{hA_s}$$

$$T_g = T_b + \frac{\varepsilon\sigma}{h}(T_b^4 - T_{surr}^4) + \Delta_{cond} + \Delta_{cat}$$

Uncertainty in gas temperature (T_g) is calculated from quadratic sum of the uncertainties [43]:

$$dT_g = \left[\left(\frac{\partial T_g}{\partial T_b}dT_b\right)^2 + \left(\frac{\partial T_g}{\partial \varepsilon}d\varepsilon\right)^2 + \left(\frac{\partial T_g}{\partial h}dh\right)^2 + \left(\frac{\partial T_g}{\partial \Delta_{cond}}d\Delta_{cond}\right)^2 + \left(\frac{\partial T_g}{\partial \Delta_{cat}}d\Delta_{cat}\right)^2\right]^{1/2}$$

$$dT_g = \left[\left[\left(1 + \frac{4\varepsilon\sigma T_b^3}{h}\right)dT_b\right]^2 + \left[\frac{\sigma}{h}\left(T_b^4 - T_{surr}^4\right)d\varepsilon\right]^2 + \left[-\frac{\varepsilon\sigma}{h^2}\left(T_b^4 - T_{surr}^4\right)dh\right]^2 + d\Delta_{cond}^2 + d\Delta_{cat}^2\right]^{1/2}$$

Convective heat transfer coefficient is defined as:

$$h = \frac{k_{air}Nu}{d_b}$$

$$dh = \left[\left(\frac{\partial h}{\partial k_{air}} dk_{air} \right)^2 + \left(\frac{\partial h}{\partial Nu} dNu \right)^2 + \left(\frac{\partial h}{\partial d_b} dd_b \right) \right]^{1/2}$$

$$dh = \left[\left(\frac{Nu}{d_b} dk_{air} \right)^2 + \left(\frac{k_{air}}{d} dNu \right)^2 + \left(\frac{-k_{air} Nu}{d_b^2} dd_b \right) \right]^{1/2}$$

Assuming that for a certain temperature, $dk_{air} = 0$ and $dNu = 0$ we have:

$$dT_g = \left[\begin{array}{l} \left[\left(1 + \frac{4\varepsilon\sigma T_b^3 d_b}{k_{air} Nu} \right) dT_b \right]^2 + \left[\frac{\sigma d_b}{k_{air} Nu} \left(T_b^4 - T_{surr}^4 \right) d\varepsilon \right]^2 + \left[-\frac{\varepsilon\sigma}{k_{air} Nu} \left(T_b^4 - T_{surr}^4 \right) dd_b \right]^2 \\ + d\Delta_{cond}^2 + d\Delta_{cat}^2 \end{array} \right]^{1/2}$$

The uncertainty in T_b measured by the thermocouple is taken to be 0.25% of the measured temperature, the average uncertainty in the ε is taken to be 20 % , with a maximum uncertainty of 27% and a minimum of 9% which are based on the accuracy of the IR camera in measuring temperature (2% of measured temperature). The accuracy of defining the diameter of the bead is on average taken as 15%.

Bibliography

[1] Turns, S. R., *An Introduction to Combustion, Concepts and Applications*, Second Edition, McGraw-Hill Company, New York, 2000.

[2] Karim, G. A., "Hydrogen as a Spark Ignition Engine Fuel", *International Journal of Hydrogen Energy*, Vol. 28, pp. 569-577, 2003.

[3] Schefer, R. W., "Hydrogen Enrichment for Improved Lean Flame Stability", *International Journal of Hydrogen Energy,* Vol. 28, pp. 1131-1141, 2003.

[4] Kostiuk, L. W., Bray, K. N. C., and Chew, T. C., " Premixed Turbulent Combustion in Counterflowing Streams", *Combustion Science and Technology*, Vol. 64, pp. 233-241, 1989.

[5] Plaia , J. M., Ph.D. Thesis, University of Maryland, College Park, 2005

[6] Glassman, I., *Combustion*, Second Edition, Academic Press, INC., pp. 111-114, 1987.

[7] Law, C. K., and Sung, C. J., "Structure, Aerodynamics, and Geometry of Premixed Flamelets", *Progress in Energy and Combustion Science*, Vol. 26, pp. 459-505, 2000.

[8] Law, C. K., "Dynamics of Stretched Flames", *Twenty-Second Symposium (International) on Combustion*, The Combustion Institute, pp. 1381-1402, 1988.

[9] Luff, D., Korusoy, E., Lindstedt, P. and Whitelaw, J. H., "Counterflow Flames of Air and Methane, Propane and Ethylene, with and without Periodic Forcing", *Experiments in Fluids*, Vol. 35, pp. 618-626, 2003

[10] Law, C. K., Zhu, D. L., and Yu, G., "Propagation and Extinction of Stretched Premixed Flames", *Twenty-first Symposium (International) on Combustion*, The Combustion Institute, pp. 1419-1426, 1986.

[11] Ishizuka, S., and Law, C. K., "An Experimental Study on Extinction and Stability of Stretched Premixed Flames", *Nineteenth Symposium (International) on Combustion*, The Combustion Institute, pp. 327-335, 1982.

[12] Cheng, Z., Wehrmeyer, J. A., and Pitz, R. W., "Lean or Ultra Lean Stretched Planar Methane/Air Flames", *The 30th Proceedings of the Combustion Institute*, 2004.

[13] Sato, J., "Effects of Lewis Number on Extinction Behavior of Premixed Flames in a Stagnation Flow", *Nineteenth Symposium (International) on Combustion*, The Combustion Institute, pp. 1541-1548, 1982.

[14] Chen, Z. H., and Sohrab, S. H., "Flammability Limit and Limit Temperature of Counterflow Lean Methane-Air Flames", *Combustion and Flame*, Vol. 102, pp. 193-199, 1995.

[15] Korusoy, E., and Whitelaw, J. H., "Extinction and Relight in Opposed Flames", *Experiments in Fluids*, Vol. 33, pp. 75-89, 2002.

[16] Tsuji, H., and Yamaoka, I., "Structure and Extinction of Near-limit Flames in a Stagnation Flow", *Nineteenth Symposium (International) on Combustion,* The Combustion Institute, pp. 1533-1540, 1982.

[17] Jackson, G. S., Sai, R., Plaia, J. M., Boggs, C. M., and Kiger, K. T., "Influence of H_2 on the Response of Lean Premixed CH_4 Flames to High Strained Flows", *Combustion and Flame*, Vol. 132, pp. 503-511, 2003.

[18] Yu, G., Law, C. K., and Wu, C. K., "Laminar Flame Speed of Hydrocarbon + Air Mixtures with Hydrogen Addition", *Combustion and Flame*, Vol. 63, pp. 339-347, 1986.

[19] Sardi, K., Taylor, A. M. K. P., and Whitelaw, J. H., "Extinction of Turbulent Counterflow Flames under Periodic Strain", *Combustion and Flame*, Vol. 120, pp. 265-284, 2000.

[20] Logue, J. M., "Characteristics of Low Strain Near Extinction Flames in μG and 1G", M.S. Thesis, University of Maryland, College Park, 2003.

[21] Law, C. K, Sung, C. J., Yu, G., and Axelbaum, R. L., "On the Structural Sensitivity of Purely Strained Planar Premixed Flames to Strain Rate Variations", *Combustion and Flame*, Vol. 98, pp. 139-154, 1994.

[22] Shaddix, C. R., "Practical Aspects of Correcting the Thermocouple Measurements for Radiation Loss", Combustion Research Facility, Sandia National Laboratories, WSS/CI 98F-24, 1998.

[23] Smooke, M. D., Puri, I. K., and Seshadri, K., "A Comparison Between Numerical Calculations and Experimental Measurements of the Structure of a Counterflow Diffusion Flame Burning Diluted Methane in Diluted Air", *Twenty-First Symposium (International) on Combustion*, The Combustion Institute, pp. 1783-1792, 1986.

[24] Cong, Y., "The Effects of Hydrogen Doping on Lean Stability of Premixed Methane Flames", M.S. Thesis, University of Maryland, College Park, 1999

[25] Sai, R., "A Study on Effects of H_2 Addition To Highly Strained Lean Premixed Laminar Methane and Propane Flames", M.S. Thesis, University of Maryland, College Park, 2003

[26] Burton, K. A., Ladouceur, H. D., and Fleming, J. W., "An Improved Noncatalytic Coating for Thermocouples", *Combustion Science and Technology*, Vol. 81, pp. 141-145, 1992.

[27] Marshall, A. W., "Effects of Jet Momentum Distribution on Combustion Characteristics in Co-swirling Flames", Ph.D. Thesis, University of Maryland, College Park, 1996.

[28] Cardanelli, F., *Materials Handbook, A Concise Desktop Reference*, Springer-Verlog, London, pp. 314, 2000

[29] Whitaker, S., "Forced Convection Heat Transfer Correlations for Flow in Pipes, Past Flat Plates, Single Cylinders, Single Spheres, and for Flow in Packed Beds and Tube Bundles", *AlChE Journal*, Vol. 18, No. 2, pp. 361-371, 1972

[30] Incropera, F. P., and DeWitt, D. P., *Fundamentals of Heat and Mass Transfer*, Fifth Edition, John Wiley and Sons, 2002.

[31] Heitor, M. V., and Moreira, A. L. N., "Thermocouple and Sample Probes for Combustion Studies", *Progress in Energy and Combustion Science*, Vol. 19, pp. 259-278, 1993.

[32] Bradley, D., and Mattews, K. J., "Measurement of High Gas Temperatures with Fine Wire Thermocouples", *Journal Mechanical Engineering Science*, Vol. 10, No. 4, pp. 299-305, 1968

[33] Petit, C., Gajan, P., Lecordier, J. C., and Parantheon, P., "Frequency Response of Fine Wire Thermocouple", *Journal of Physics E: Scientific Instruments*, Vol. 15, pp. 760-764, 1982.

[34] Fristrom, R. M., *Flame Structure and Processes*, Oxford University Press, Inc., 1995.

[35] Blevins, L. G., and Pitts, W. M., "Modeling of Bare and Aspirated Thermocouples in Compartment Fires", *Fire Safety Journal*, Vol. 33, pp. 239-259, 1999.

[36] Drysdale, D. D., *An Introduction to Fire Dynamics*, Second Edition, John Wiley and Sons, pp. 65-69, 1998.

[37] Gray, W. A., and Muller, R., *Engineering Calculations in Radiative Heat Transfer*, Pergamon Press, Oxford, pp. 70-75, 1974

[38] Welty, J. R., Wilson, R. E., and Wicks, C. E., *Fundamentals of Momentum, Heat and Mass Transfer*, Second Edition, John Wiley and Sons, New York, pp. 457-461, 1976.

[39] Pollock, D. D., *Thermocouples*: *Theory and Properties*, CRC Press, Inc., pp. 220-222, 1991.

[40] Aghalayam, P., Park, Y. K., Fernandes, N., Papavassiliou, V., Mhadeshwar, A. B., and Vlachos D. G., "*A C1 Mechanism for Methane Oxidation on Platinum*", Journal of Catalysis, Vol 213, pp. 23-38, 2003.

[41] Weckmann, S., "Dynamic Electrothermal Model of a Sputtered Thermopile Thermal Radiation Detector for Earth Radiation Budget Applications", M.S. Thesis, Virginia Polytechnic Institute and State University, 1997

[42] Bradley, D., Lau, A. K. C., and Missaghi, M., "Response of Compensated Thermocouple to Fluctuating Temperatures: Computer Simulation, Experimental Results and Mathematical Modeling", *Combustion Science and Technology*, Vol. 64, pp. 119-134, 1989

[43] Taylor, J. R., *Introduction to Error Analysis, Study of Uncertainties in Physical Measurements*, Oxford University Press, pp. 40-73, 1982